

Artificial Vasa-Vasorum Serves as an On-Site Regenerative Promoter of Cell-Free Vascular Grafting

주저자 논문, Acknowledgements에 표기되어 있음.

Hyun-su Ha, Sewoom Baek, **Kyubae Lee**, Sungwoo Cho, Min Jeong Cho, Seyong Chung, Hyeongyun Choi, Chan Hee Lee, Min Seok Kim, Si Yeong Kim, Dae-Hyun Kim, Sang-Wook Kang,* and Hak-Joon Sung*

The control paradigm of small vessel pathophysiology has changed to focus on the vascular out-wall rather than the lumen-intimal factors. As an emerging controller of the external wall, the microvasculature (“vasa vasorum”) provides interactional routes between the in-and out-sides of the vascular wall. Despite numerous approaches to developing small-diameter vascular grafts, engineering artificial vasa vasorum (AVV) has not been projected as a multi-functional solution to address long-standing issues such as thrombotic and immune controls for wall regeneration. Here, the AVV is engineered using a microchannel network hydrogel after a multi-study validation of implantation functions and then used to wrap the external wall of the cell-free vessel post-decellularization while preserving its mechanical properties. Upon inter-positional and bypass grafting to rabbit arteries, the AVV graft facilitates the recruitment of vascular cells into the cell-free wall by promoting invasion of angiogenic and vasculogenic cells through the microchannel-mediated M2 polarization of macrophages. This function results in the efficient restoration of smooth muscle cells, and the revitalized vascular elasticity helps to maintain long-term patency. The AVV, therefore, serves as an effective catalyst for vascular wall regeneration, offering a solution to clinically successful small-diameter vascular grafting.

endothelial progenitor cells (EPCs), myeloid cells (e.g., monocytes), and hemodynamics as brain factors to operate the smooth muscle contraction and adventitial scaffolding.^[2] A recent paradigm of research has been shifted to accept the outside-in control because studies have reported that adventitial microvascular network (“vasa-vasorum”) and pericytes with the characteristics of mesenchymal stem cells (MSCs) can guide vascular regeneration and pathophysiology.^[3] The vasa-vasorum is explained as the vessel of vessels, which is formed as a dense microvascular network in the arterial adventitia.^[4] Vasa-vasorum not only supplies blood with nutrients and oxygen to the artery but also regulates vascular pathophysiology including inflammation, stenosis, and regeneration. Another key function is to provide interactional routes throughout the vascular wall for cells to replace, restore, and regenerate from the adventitial side, indicating a key outside-in controller of

the heterogeneous cell activities within the arterial tissue.^[5] Indeed, impaired functions of vasa-vasorum often result in graft failure with stenotic wall remodeling due to the ischemic disorders of cellular functions.^[6]

Morphological changes of cells direct differentiation and phenotypic alternation.^[7] Each cell type has unique plasticity such as contractile versus migratory phenotype of vascular smooth muscle cells (VSMCs),^[8] cobblestone versus spindle

1. Introduction

Cells grow into tissues through vascular networks and thereby serve as heterogeneous functional players under a harmonized operation.^[1] Multiple cell types reside in arterial tissue through recruitment from the luminal (inside-out) and adventitial (outside-in) sides. For the past decades, the inside-out control has been studied with a focus on endothelial cells (ECs),

H.-su Ha, K. Lee, S. Cho, S. Chung, H. Choi, C. H. Lee, M. S. Kim, S. Y. Kim, H.-J. Sung
Department of Medical Engineering
Yonsei University College of Medicine
50-1 Yonsei-ro, Seodaemun-gu, Seoul 03722, Republic of Korea
E-mail: hj72sung@yuhs.ac

 The ORCID identification number(s) for the author(s) of this article can be found under <https://doi.org/10.1002/adfm.202315310>

© 2024 The Authors. Advanced Functional Materials published by Wiley-VCH GmbH. This is an open access article under the terms of the [Creative Commons Attribution-NonCommercial-NoDerivs](#) License, which permits use and distribution in any medium, provided the original work is properly cited, the use is non-commercial and no modifications or adaptations are made.

DOI: 10.1002/adfm.202315310

S. Baek, H.-J. Sung
Department of Brain Korea 21 FOUR Project for Medical Science and Medical Engineering
Yonsei University College of Medicine
50-1 Yonsei-ro, Seodaemun-gu, Seoul 03722, Republic of Korea
K. Lee
Department of Biomedical Materials
Konyang University
158, Gwanjeodong-ro, Seo-gu, Daejeon 35365, Republic of Korea

phenotype of ECs,^[9] and myogenic versus non-myogenic phenotype of fibroblasts.^[10] A variety of 2D and 3D patterns in culture substrates have been explored to prove that the morphological change can be induced using a pattern to guide the phenotype alternation of plastic cells.^[11] As a multi-functional operator of vascular homeostasis, macrophages undergo destructive M1 or regenerative M2 polarization upon the phenotypic alternation.^[12] In particular, monocytes have been reported to possess EPC characteristics in conjunction with angiogenic M2 polarization.^[13] Hence, this regenerative characteristic can be promoted by forcing tight cell-cell adhesion like ECs when monocytes are packed in alignment using a specific 3D structure such as microchannels. The regenerative polarization of macrophages promotes angiogenesis by recruiting ECs and EPCs as well as differentiation of pericytes or MSCs to SMCs through a transforming growth factor (TGF)- β mechanism.^[14]

Continuous progress has been made in developing a small-diameter arterial graft (< 6 mm). However, unmet needs remain in implementing the elastic and scaffolding properties of graft walls through tissue regeneration upon restoration of vascular cells, in addition to addressing the thrombosis issue due to the small size.^[15] As the most popular strategy, synthetic and natural polymers have been used to produce a tube scaffold with in vitro culturing or in vivo recruiting of vascular cells so that cellularization of the scaffold can lead to natural tissue production as the scaffold degrades.^[16] Another important issue to address is that the impaired balances in the compositional heterogeneities of vascular cells and extracellular matrix (ECM) result in graft failures.^[17] Moreover, successful grafting requires the rate alignment of host cell growth and ECM production with scaffold degradation. In this regard, the preservation of ECM balance by decellularized vessels is considered a key advantage because the cellularization into balanced composition does not require scaffold degradation and ECM production.^[18] The balanced ECM composition of decellularized vessels can act as an on-site recruiter of each host cell type to the corresponding tissue layer in vivo even when the decellularized vessel ("cell-free") is implanted.

In this study, artificial vasa-vasorum (AVV) is engineered within an implantable hydrogel by generating microchannel networks in the similarities of structure and size to those of vasa-vasorum. As an allograft concept, a rabbit carotid artery is decellularized by testing the well-known methods to preserve the intact ECM content such as collagen and glycosaminoglycan (GAG). The graft is fabricated by producing the AVV to wrap the outer wall of the cell-free scaffold in a customized mold and subjected

to heparin immobilization without any cell culture. In this way, on-site recruitment of vascular cells is approached upon grafting while preventing thrombotic responses to blood flow. The AVV facilitates efficient diffusion and perfusion in vitro and in vivo with a successful result of in vitro endothelialization by preserving cell viability when induced pluripotent cell-derived ECs (iPSC-ECs) invade into the channel networks for 7 days. When the graft is interposed into a rabbit carotid artery with a diameter similar to that of a human coronary artery (< 3 mm) using end-to-end anastomosis for 30 days, the AVV effect becomes clearer in maintaining the flow patency by suppressing stenotic wall remodeling with preservation of arterial flow rate as opposed to the channel-free graft control. The AVV promotes invasion of E(P)Cs and monocytes from both adventitial and luminal sides into the cell-free scaffold with increases in the expression of angiogenic genes in the E(P)Cs. As a key mechanism, AVV induces M2 polarization of macrophages by packing in alignment like ECs through the channel structure. This mechanism drives i) the inside-out and outside-in endothelialization and ii) the restoration of SMCs by promoting MSC differentiation through TGF- β production, leading to recovery of scaffold elasticity. The promising function to maintain graft patency is confirmed by the femoral artery interposition (< 1 mm diameter) and iliac artery-to-aorta bypass (> 3 mm diameter) models in rabbits. The present approach suggests a previously unconsidered solution to move toward the success of small vessel grafting for clinical translation.

2. Result

2.1. Production and Characterization of AVV

AVV is produced as a dense microchannel network within microbial transglutaminase (mTG) cross-linkable gelatin hydrogel, which wraps a decellularized ("cell-free") vascular scaffold (Figure 1a). As the generator of microchannel network in AVV, a thread of poly (N-isopropyl acrylamide) (pNIPAM) microfibers exhibits a typical diameter distribution of microvasculature (5 – 25 μm) with an average of $14.94 \pm 5.81 \mu\text{m}$ (Figure S1a,b, Supporting Information). The pNIPAM fibers are embedded in mTG hydrogel with crosslinking at 37 °C, followed by melting the fibers through gel-to-sol transition at room temperature below low critical solution temperature (32 °C), thereby generating void microchannel networks within the hydrogel upon perfusion washing with phosphate-buffer saline (PBS). As an indication of microchannel generation, pores within the AVV hydrogel are identified in contrast to no void pores of the channel (-) hydrogel (Figure S1c, Supporting Information). Cell-free scaffolds are produced by harvesting carotid arteries from rabbits with decellularization in comparison between mechano-chemical and chemico-chemical methods (Figure S2a, Supporting Information). The chemico-chemical method is set to perfuse chemicals continuously into the lumen of the carotid artery in a bioreactor, which is processed from 48-h treatment of sodium dodecyl sulfate (SDS) to 12-h exposure to a non-ionic detergent (Triton X-100). The mechano-chemical method starts with freezing and thawing the artery at –80 °C and 37 °C, respectively, in PBS for ten cycles, followed by perfusing Triton X-100 for 12 h in the bioreactor. All samples are lyophilized for storage.

M. J. Cho
Department of Clinical Pharmacology & Therapeutics
the Catholic University of Korea
Seoul St. Mary's Hospital
222, BanpoDaero, Seocho-gu, Seoul 06591, Republic of Korea
D.-H. Kim
Department of Veterinary Surgery
Chungnam National University College of Veterinary Medicine
99, Daehak-ro, Yuseong-gu, Daejeon 34134, Republic of Korea
S.-W. Kang
Department of Surgery
Yonsei University College of Medicine
Seoul 03722, Republic of Korea
E-mail: oralvanco@yuhs.ac

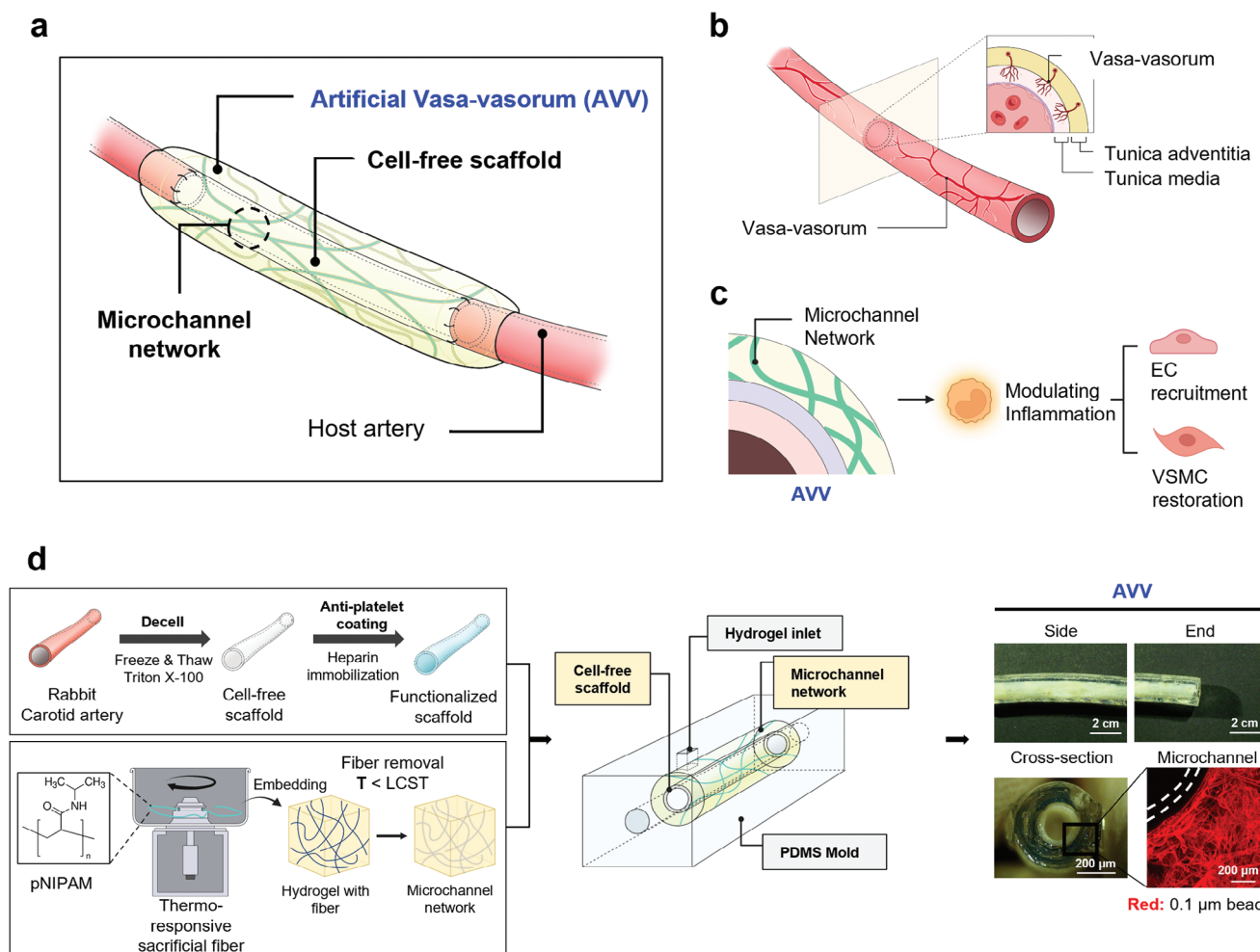


Figure 1. Introduction to artificial vasa-vasorum (AVV) with cell-free scaffold. Vasa vasorum (“vessels of vessels”) is formed as a dense microvascular network in the arterial adventitia. Vasa vasorum not only supplies blood with nutrients and oxygen to the artery but also regulates vascular pathophysiology. a) AVV is produced as a dense microchannel network within a hydrogel, which wraps a cell-free arterial scaffold. b) AVV also enables external blood supply from surrounding tissues into the adventitia and media with oxygen and nutrient transport. c) The microchannel network of AVV is proposed to induce cell invasion from the surrounding tissue into the vascular wall, which modulates inflammatory mechanisms to promote regenerative responses. The recruitment of endothelial progenitor cells (EPCs) promotes the luminal reendothelialization of intima and the microvasculature formation of adventitia, thereby enabling cellularization and functionalization of the cell-free scaffold. AVV promotes the M2 polarization of invading macrophage and the differentiation of perivascular MSCs into VSMCs with elasticity recovery. d) The scaffold is produced by decellularizing a rabbit carotid artery, followed by immobilization of anti-coagulate heparin. AVV is constructed by generating a microchannel network in a gelatin hydrogel after a dense fiber network of pNIPAM is spun and embedded in the hydrogel, followed by fiber removal upon lowering the temperature. In a 3D-printed PDMS mold, the fiber network is placed around the scaffold wall, and the hydrogel is injected onto the scaffold to cover the fiber uniformly with crosslinking, thereby producing the assembled form of AVV and scaffold upon fiber melting. (These figures were created with Biorender.com).

Decellularized vascular scaffolds have shown promising outcomes in pre-clinical studies.^[19] Both methods decellularize the arteries effectively when the vessel tissues are imaged after staining with hematoxylin and eosin (H&E) in addition to the nucleus counter-staining using 4',6-diamidino-2-phenylindole (DAPI) (Figure S2b, Supporting Information), which is further evidenced by the absence of DNA contents (Figure S2c, Supporting Information). The western blot analyses also confirmed the successful removal of cells (β -actin) including EC (CD31) and VSMC (α SMA) while preserving the α -1 type 1 collagen component of ECM (Figure S2d, Supporting Information). Compared to the chemico-chemical method, the mechano-chemical

process results in the preservation of more sulfated glycosaminoglycan (sGAG) in the ECM (Figure S2e, Supporting Information). When the mechanical properties of decellularized arteries are examined, the arterial stress-strain relationship is interpreted using the theory that the elastin-dominant tunica media handles the max strain, while the major ECM (collagen + GAG) – dominant adventitia maintains the tensile strength and tangent modulus (Figure S3a, Supporting Information). Both decellularization methods decrease the max strain compared to the native artery, indicating altered elastin functions (Figure S3b,c, Supporting Information). However, the mechano-chemical method manages the tangent modulus and ultimate tensile strength up

to those of native arteries compared to the chemico-chemical method.

AVV also mediates blood supply from surrounding external tissues into the adventitia and media, thereby supplying oxygen and nutrients to resident vascular cells (Figure 1b). Hence, the microchannel networks of AVV are proposed to serve as a route for cell invasion into the vascular wall, which modulates inflammation to promote regenerative cellular responses (Figure 1c). As a result, the recruitment of EPCs from the lumen promotes intimal reendothelialization, while E(P)C invasion through vasa-vasorum results in microvasculature formation of adventitia, thereby enabling cellularization and functionalization of the cell-free scaffold. AVV promotes M2 polarization of invading macrophage and drives differentiation of pericyte and resident MSCs into VSMCs with elasticity recovery. The scaffold is produced by decellularizing a rabbit carotid artery, followed by immobilization of anti-coagulate heparin (Figure 1d). AVV is constructed by generating microchannel networks in the mTG hydrogel. Clumps of pNIPAM fiber are spined and placed to cover the scaffold wall in a 3D-printed polydimethylsiloxane (PDMS) mold. Then, mTG hydrogel solution is injected onto the scaffold to embed the fiber uniformly upon crosslinking at 37 °C for 30 mins, followed by decreasing temperature to 32 °C (LCST) with PBS perfusion to remove the fibers. In this way, an assembled form of AVV and scaffold is produced, as evidenced by the AVV layer onto the cell-free scaffold with the clear perfusion staining of microchannels using microbeads (0.1 μm , red).

2.2. AVV as an Outside-In Route for Diffusion, Perfusion, and Invasion

AVV serves as microchannel pathways for cellular invasion with blood perfusion to transport diffusive oxygen and nutrients into the scaffold wall (Figure 2a) as evidenced by the void channel spaces onto the cell-free scaffold (microscope images) with perfusion staining of FluoSphere (0.1 μm , red) (Figure 2b). When microbeads (2 μm , red) are perfused, and fluorescein isothiocyanate (FITC)-dextran (40 kDa, green) is diffused (Figure 2c), the confocal images (0, 10, and 30 min) confirm that the microchannel network of AVV facilitates the perfusion (red) and diffusion (green) in contrast to the channel (-) group as supported by the quantitative analysis in the graphs. These findings suggest effective control over gel stiffness and channel interconnection. Dextran is a small molecule (40 kDa) that can diffuse from the microchannel into the hydrogel over the 200- μm diffusion limit^[20] without leaking from the channel network as previously reported.^[21] The time-lapse fluorescence images capture the FITC-dextran diffusion process, demonstrating the capability of microchannel networks to transport nutrients and oxygen across the external wall.

Heparin is immobilized onto the surfaces of cell-free scaffold as a means of anti-thrombotic functionalization through a tissue-friendly, and simple reaction using 1-ethyl-3-(3-dimethyl aminopropyl) carbodiimide (EDC) and N-hydroxysuccinimide (NHS). This method is compared with the coating means by soaking onto the cell-free scaffolds and no heparinized graft (control) (Figure S4a, Supporting Information). Both coating methods exhibit evidence of heparinization as opposed to the control, but more heparin remains by the immobilization compared to the soaking in

the images of toluidine blue O (TBO) staining with quantitative analysis in the graph. Compared to the (-) heparin control, the heparin immobilization results in significant reductions in both adhesion (Figure S4b, Supporting Information) and thrombotic activation of platelets as appeared with spindle shapes (Figure S4b, Supporting Information).

After heparin immobilization, the graft (AVV+ scaffold) is surgically interposed into a rabbit carotid artery for 14 days, harvested, and subjected to the perfusion and diffusion tests for 30 mins (Figure 2d). The microbeads (2 μm , red) are perfused effectively with clear dextran (40 kDa, green) diffusion in AVV in contrast to the channel (-) group. As an in vitro confirmation, induced pluripotent stem cell-derived (iPSC)-ECs are seeded onto the graft for 7 days and subjected to a live/dead assay (Figure 2e). Consequently, iPSC-ECs dominantly migrate into the AVV microchannel network in contrast to the poor cellular invasion in the channel (-) group, indicating that AVV facilitates the luminal endothelialization of microchannels. Live iPSC-ECs invade dominantly into AVV compared to the 25% increase in dead cells of the channel (-) group as supported by the quantitative analyses of cell viability with the agreement to the cellularity. The iPSC-EC viability is reduced by 25% post 7-day culture in the channel (-) group because the gel thickness is ranged to 1 mm over the 200 μm diffusion limit.^[21] Therefore, oxygen and nutrients are not sufficiently provided without the void, interconnected channel network for 7 days, which appears to play a major role in altering the cell viability considering that the gel stiffness and composition are compatible with cell culture under embedding as reported previously.^[20]

2.3. Patent Carotid Artery by AVV Post Rabbit Interposition Grafting

Each graft group is surgically interposed into a right carotid artery (1.5–2.0 mm in diameter) in rabbits for 30 days through end-to-end anastomosis (Figure 3a). The proximal anastomosis site of the graft was harvested and analyzed because this site is prone to stenosis and thrombosis by blood flow disturbance.^[22] The scaffold-only group without hydrogel wrapping serves as a control for 14 days with analyses by histology and Doppler ultrasound (US), and AVV is compared with the channel (-) group on days 7, 14, and 30 by Doppler US, angiography, histology, and qPCR (Figure 3b). First, the scaffold only control exhibits the stenotic obstruction with heavy thrombosis and neointima formation in the H&E images, resulting in the poor patency rate (0–0.2 m s^{-1}) under US doppler imaging (Figure S5, Supporting Information). Vascularization into AVV is seen as opposed to the channel (-) group under macroscopic imaging on day 14 post-surgery (Figure 3c) as further supported by the clear patency of AVV in contrast to the flow occlusion of the channel (-) group upon angiography on day 30 post-surgery (Figure 3d). In the H&E analyses (Figure 3e; Figure S6, Supporting Information), the channel (-) group exhibits heavy luminal thrombosis (Day 7), neointima formation (Day 14), and luminal occlusion with wall shrinkage and gel degradation in addition to neointima (Day 30) compared to the maintenance of intact patency and structure in AVV. These results are confirmed by quantitative analyses of the lumen area with the histological finding of thrombosis and

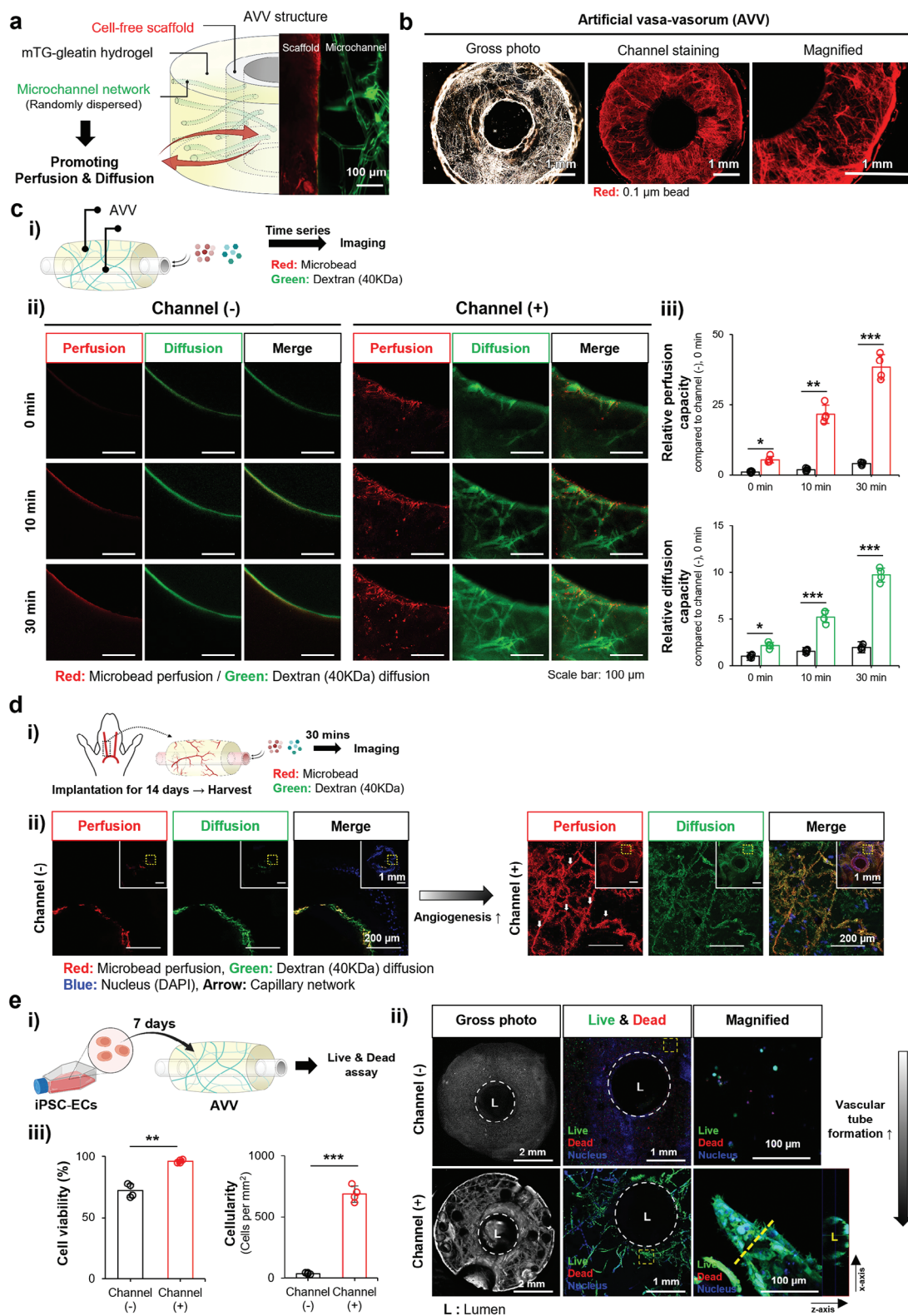


Figure 2. AVV is an outside-in route for diffusion, perfusion, and invasion. a) AVV serves as inter-connected microchannel pathways (green) in random dispersion throughout the hydrogel for cellular invasion with blood perfusion to transport diffusive oxygen and nutrients into the scaffold wall (red) as evidenced by b) perfusion staining of FluoSphere (0.1 μ m, red) with the gross photo image. c) i) When microbeads (2 μ m, red) are perfused, and FITC-dextran (40 kDa, green) is diffused, ii) the confocal images (0, 10, and 30 min) confirm that the microchannel network of AVV facilitates perfusion and diffusion in contrast to the channel (-) group as supported iii) by the quantitative analysis. d) i) When the graft (AVV+ scaffold) is surgically interposed

neointima. Of note, the variations of hydrogel texture appear i) due to gelatin denaturation resulting from the heat generation through paraffin embedding. This variation is similar between AVV and the channel (-) group as the channel structure disappears through the gel denaturation. AVV maintains the healthier patterns of pulsatile flow with the sharper, higher forward peak with the minimal backflow compared to the channel (-) group for 30 days in the Doppler US (Figure 3f), which is further confirmed by the quantitative analysis of the peak flow rate (Figure 3g). Consequently, endothelialization of vasa vasorum is induced by the microchannel structure (Figure S7, Supporting Information). After interposition grafting for 30 days, rabbit carotid arteries with the grafts are harvested and analyzed. The AVV microstructure promotes vascularization and CD31 expression with consequent increases in the vessel number in tunica media and adventitia compared to the channel (-) group.

2.4. Pro-Endothelialization by AVV Through Regenerative Macrophage Polarization

The channel (-) group induces thrombosis (Day 7) and neointima formation (Day 14) in the absence of endothelialization (CD31) and monocyte invasion (CD11b) (Figure 4a), which are prevented by AVV with endothelialization and monocyte invasion from the lumen to intima (inside-out, day 7) and from AVV on adventitia to media (outside-in, day 14) as confirmed by the protein expression of CD31 and CD11b (Figure 4b). As hypotheses (Figure 4c), EPCs are recruited from the luminal blood to intima (inside-out) first, and then, E(P)Cs invades through AVV on adventitia into media (outside-in), thereby preventing thrombosis and neointima formation. These regenerative actions of E(P)Cs are synergized by M2 polarization of monocytes upon invasion with channel packing in alignment. Compared to the channel (-) group on day 7 post-implantation, AVV significantly promotes the expression of the M2 marker (ARG-1) in monocytes as opposed to the M1 marker (iNOS) within the scaffold walls (Figure S8, Supporting Information). Indeed, AVV promotes the marker gene expression of EC (CD31) and EPC (CD34 and 133) compared to the channel (-) group (Figure 4d). The CD31 expression is dominantly promoted on day 14 in contrast to the peak expression of CD34 and CD133 on day 7.

The microchannel network drives the EC-mimetic packed lining of macrophages with M2 polarization. Macrophages (Raw264.7) are seeded in the test hydrogels for 2 days and subjected to inflammatory LPS activation for 5 more days, followed by immunocytochemistry (ICC) and PCR analyses on day 7 (Figure S9a, Supporting Information). When Raw264.7 cells are cultured on the channel (+) versus (-) hydrogels (Figure S9b, Supporting Information), cell packing in alignment through the channels is seen in contrast to cell clumping in the channel (-) hy-

drogel. As opposed to the channel (-) group (Figure S9c, Supporting Information), the channel (+) group promotes the protein expression of M2 maker [Arginase (ARG)-1] with suppression of M1 marker [inducible nitric oxide (iNOS)] expression (Figure S9d, Supporting Information), which is confirmed by the quantitative analysis (Figure S9e, Supporting Information). The results are further supported by the channel-mediated significant decreases in the gene expression of M1 markers including interleukin (IL)-1B, iNOS, tumor necrosis factor (TNF)- α , and IL-6 in contrast to the significant increases in the gene expression of M2 markers including CD206, CD163, IL-10, ARG-1, and transforming growth factor (TGF)- β , compared to the channel (-) group (Figure S9f, Supporting Information). Compared to the channel (-) group (Figure 4e), AVV promotes monocyte invasion (CD11b) with induction of the M2 marker (ARG-1) as opposed to the M1 marker (iNOS), which is supported by the number of each monocyte type and the marker gene expression of M1 (IL-1B, TNF- α) and M2 (IL-10, ARG-1) polarization on day 14.

The M2 polarization of macrophages is promoted due to microchannel-mediated cell packing and lining, which is proposed to serve as a promoter of circulating EPCs recruited from the lumen to the scaffold as a means of inside-out endothelialization (Figure S10a, Supporting Information). Hence, macrophages (Raw264.7) are cultured under inflammatory LPS induction into the hydrogel (+/-channel), which is placed in the center of the plate (Figure S10b, Supporting Information). Then, EPCs are seeded to cover the peripheral area surrounding the hydrogel to allow for migration toward the hydrogel during the 14-day culture. The bottom of the hydrogel is denoted as a cell-free region because EPC seeding is blocked by the hydrogel or a hydrogel-size disc to produce the w/o Gel group with EPC culture without gel and macrophage. Compared to the pre-migration status (Figure S10c, Supporting Information), the channel (+) group induces EPC migration most among the test groups. The channel (-) group also promotes EPC migration, compared to the w/o Gel group. These results are confirmed by quantitative image analysis (Figure S10d, Supporting Information).

2.5. VSMC Restoration by AVV Through Regenerative Macrophage Polarization

On day 30 post-implantation into a rabbit carotid artery (Figure 5a), AVV promotes VSMC restoration into the tunica media of scaffold compared to the channel (-) group as evidenced clearly by the significant increases in the protein expression of alpha smooth muscle actin (α SMA) and myosin heavy chain (MYH)-11. AVV promotes M2 polarization of macrophages with consequent TGF- β production, which is proposed as a mechanism to drive VSMC differentiation of perivascular MSCs (Figure 5b). The image analysis of protein expression (Figure 5c)

into a rabbit carotid artery for 14 days, harvested, and subjected to the perfusion/diffusion test for 30 min, ii) the microbeads are perfused effectively with clear dextran diffusion in AVV in contrast to the channel (-) group. e) i) As an in vitro confirmation, iPSC-ECs are seeded onto the graft for 7 days and subjected to a live/dead assay. ii) Live iPSC-ECs invade dominantly into the AVV, leading to luminal endothelialization (yellow line) within the microchannels. In contrast, the channel (-) group exhibits poor cellular invasion with a 25% increase in dead cells. iii) These results are supported by the quantitative analyses of cell viability with the agreement by the cellularity (cell #/mm²). Statistical significance and p-values are determined using *t*-tests for pairwise comparisons and one-way ANOVA followed by Tukey's post hoc test for multiple groups (*N* = 4, each group, **p* < 0.05, ***p* < 0.01, ****p* < 0.001). (These figures were created with Biorender.com).

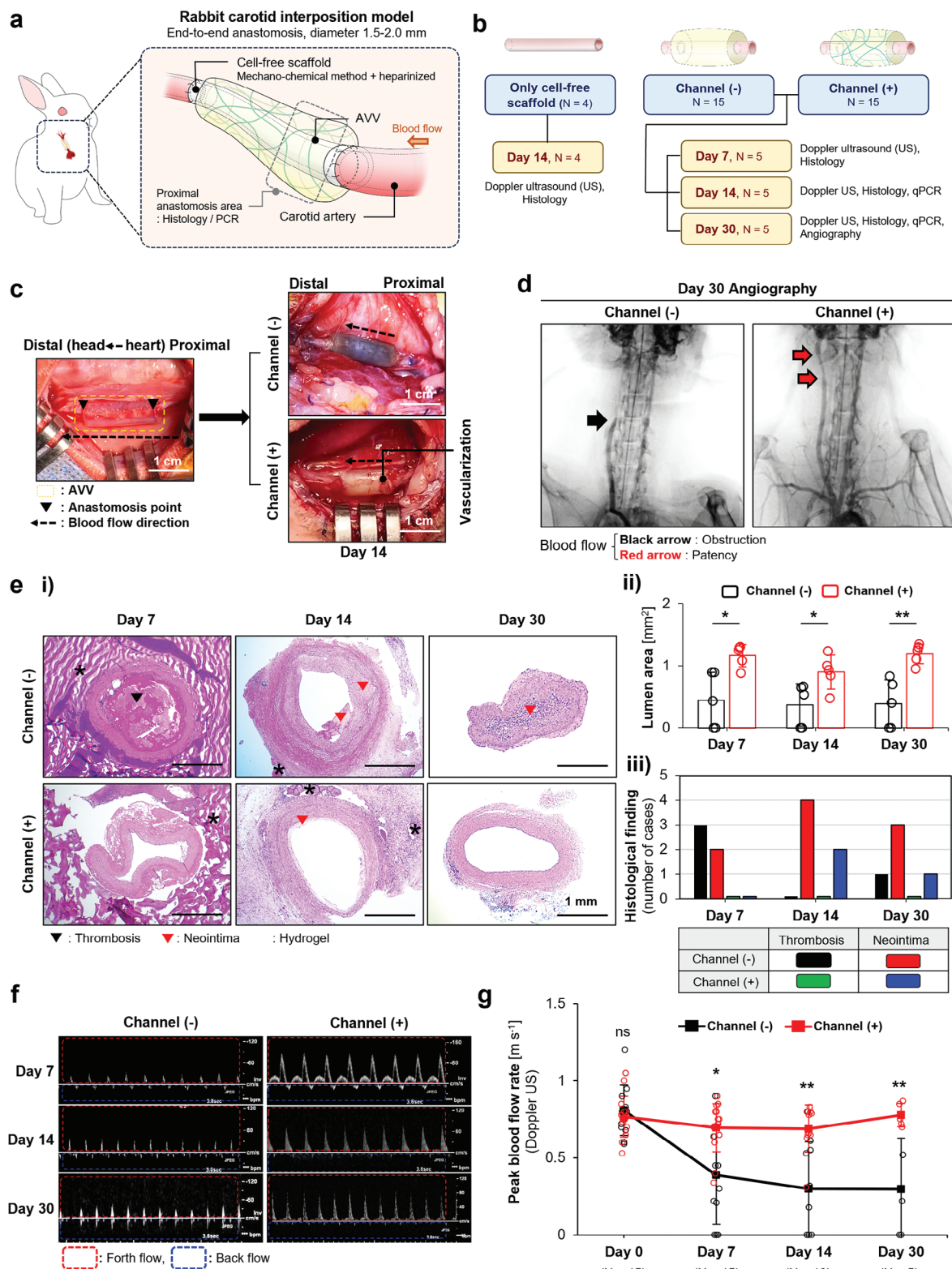


Figure 3. Patent carotid artery by AVV post rabbit interposition grafting. a) The graft (AVV + scaffold) is surgically interposed into a right carotid artery in rabbits for 30 days through end-to-end anastomosis. b) AVV is compared with the only cell-free scaffold group on day 14, channel (-) group on day 7, 14, and 30 by Doppler ultrasound (US) and histology with qPCR (Day 14 and 30) and angiography (Day 30 only). The only cell-free scaffold group as the control group performed histology and Doppler sonography on day 14. c) Vascularization into AVV is seen as opposed to the channel (-) group under macroscopic imaging on day 14 post-surgery d) as supported by the clear patency of AVV in contrast to the flow occlusion of channel (-) group upon

and the gene expression of α SMA, smooth muscle (SM)22 α , and TGF- β (Figure 5d) validates the mechanism. Compared to the channel (-) group, AVV promotes MSC invasion (CD90) on day 14 and differentiation to SMCs on day 30 as evidenced by the expression of α SMA (Figure S11, Supporting Information). In the channel (+) group, the α SMA expression gradually increases over CD90 for 30 days. In the radial tensile test of harvested graft after tube cutting (Figure 5e), AVV increases the tensile stress and strain at break significantly up to the levels of native artery compared to the channel (-) and pre-op scaffold groups despite the maintenance of modulus among the test groups. The mechanistic channel effect is determined by placing either channel (+) or (-) hydrogel on the upper trans-well chamber post Raw264.7 culture under LPS induction for 2 days (Figure 5f). MSCs are cultured at the bottom of the well for 7 days to determine differentiation to SMCs. The channel promotes α SMA expression in MSCs compared to the channel (-) group as further evidenced by the significant increases in gene expression of α SMA and SM22 α genes and the TGF- β secretion to the culture media.

2.6. Effective AVV Grafting to Vessels in ≤ 1 or ≥ 3 mm Diameter

As a microsurgical model for vessel replacement, the graft is interposed into a rabbit femoral artery (≤ 1 diameter) below the knee through end-to-end anastomosis (Figure 6a). The 14 day-implantation upon successful grafting results in microvascularization by AVV in contrast to the thrombotic colorization of channel (-) group (Figure 6b). AVV prevents neointima formation as opposed to the channel (-) group in H&E staining with agreement by the quantitative analysis of lumen area (Figure 6c). Compared to the channel (-) group (Figure 6d), AVV promotes the graft patency with the significant increase of lumen diameter under angiography, thereby generating the healthier flow patterns as evidenced by the higher peak velocity upon the Doppler US analysis (Figure 6e). As a model of bypass grafting for target vessels in ≥ 3 mm diameter (Figure 6f), the AVV scaffold is subjected to side-to-side anastomosis with bypassing from descending aorta to common iliac artery (CIA). On day 14 post-implantation of the graft (AVV + scaffold), the flow patency is maintained effectively in angiography, as further supported by the healthy pattern of high-peak pulsatile flow with a normal forward-to-backward ratio under Doppler US.

3. Discussion

All levels of biological action with organ, tissue, cell, and molecule occur in a cascade fashion, which can be applied to interpret not only pathogenesis but also regeneration. Organ functions are operated by decision-maker cells in collaboration with hardware cells. In these aspects, most therapeutic and regenerative strategies to handle the vascular pathophysiology have been

targeted to the lumen-intima side with the expectation to exert the cascade effects on the vessel wall (inside-out control). For the past decades, much less attention has been paid to the opposite direction of strategies (outside-in control). This study is aligned with this paradigm shift to focus on the vasa-vasorum of vascular out wall as an onsite recruiter of vascular cells into the cell-free scaffold.^[3,23] The regenerative actions propagate from AVV to the smooth muscle layer with the pro-endothelialization effect. The catalyst action to initiate this cascade effect is the microchannel-mediated M2 polarization of macrophages, which is effective enough to maintain the patency in the three models of small vessel grafting (< 6 mm in diameter).

The successful grafting of small-diameter vessels should maintain the efficient flow patency by facilitating endothelialization which has been approached previously by generating porous structures in the grafts using micro/nanofibers,^[24] 3D printed networks,^[25] and decellularized tissues.^[26] These approaches aim to induce the formation of microvascular-like structures (e.g., vasa vasorum) by facilitating invasion and intercellular interaction of endothelial cells which are essential for regeneration and functionalization of the vascular wall. However, the role of microvascular-like structures in vascular patency has not been clearly understood despite the meaningful previous approaches. In this aspect, the present study generates a scientific value by elucidating the mechanism by which the microchannel network in AVV induces M2 polarization of macrophages through the following process. When macrophages invade into the microchannel network whose diameter is a cell size, the migration speed decreases upon packing in alignment like a motorcade in a small tunnel. This physical setting forces M2 polarization of macrophages by mimicking EC lining in a blood vessel. Under this paradigm of structure-function relationship, macrophages are forced to adopt tight cell-cell packing due to the spatial constraint of the microchannel network. As a result, this physical altercation with the morphological adoption promotes the M2 polarization with a functional switch to vascularization^[27] as evidenced by promoting the marker expression at both protein and gene levels (Figure 4; Figures S8 and S9, Supporting Information). In this way, regenerative paracrine signals are produced to recruit E(P)Cs from both luminal and adventitial sides, resulting in endothelialization of the intima and AVV (Figure 2e; Figure S10, Supporting Information). Also, the production of TGF- β through the M2 polarization appears to cause the differentiation of precursor cells such as pericytes and MSCs to SMCs (Figure 5; Figure S11, Supporting Information), which is synergized in collaboration with endothelialization. Consequently, this mechanism serves as a functional foundation to maintain the flow patency in the three different models of small vessel grafting in vivo.

This study possesses considerable value because the easily accessible design of the AVV graft is used to validate the cascade

angiography on day 30 post-surgery. e) i) In H&E analyses, the channel (-) group exhibits heavy luminal thrombosis (Day 7), neointima formation (Day 14), and luminal occlusion (Day 30) with wall shrinkage and gel degradation in addition to neointima compared to the maintenance of intact patency and structure in AVV. ii) These results are confirmed by quantitative analyses of lumen area iii) with the histological finding of thrombosis and neointima. f) Consequently, AVV maintains the healthier patterns of pulsatile flow with the sharper, higher forward peak with the minimal backflow compared to the channel (-) group for 30 days in the Doppler US g) as confirmed by the quantitative analysis of the peak flow rate. All statistical analyses are performed using one-way ANOVA followed by Tukey's multiple comparison test (* $p < 0.05$, ** $p < 0.01$). (Figure 3a, b created with Biorender.com).

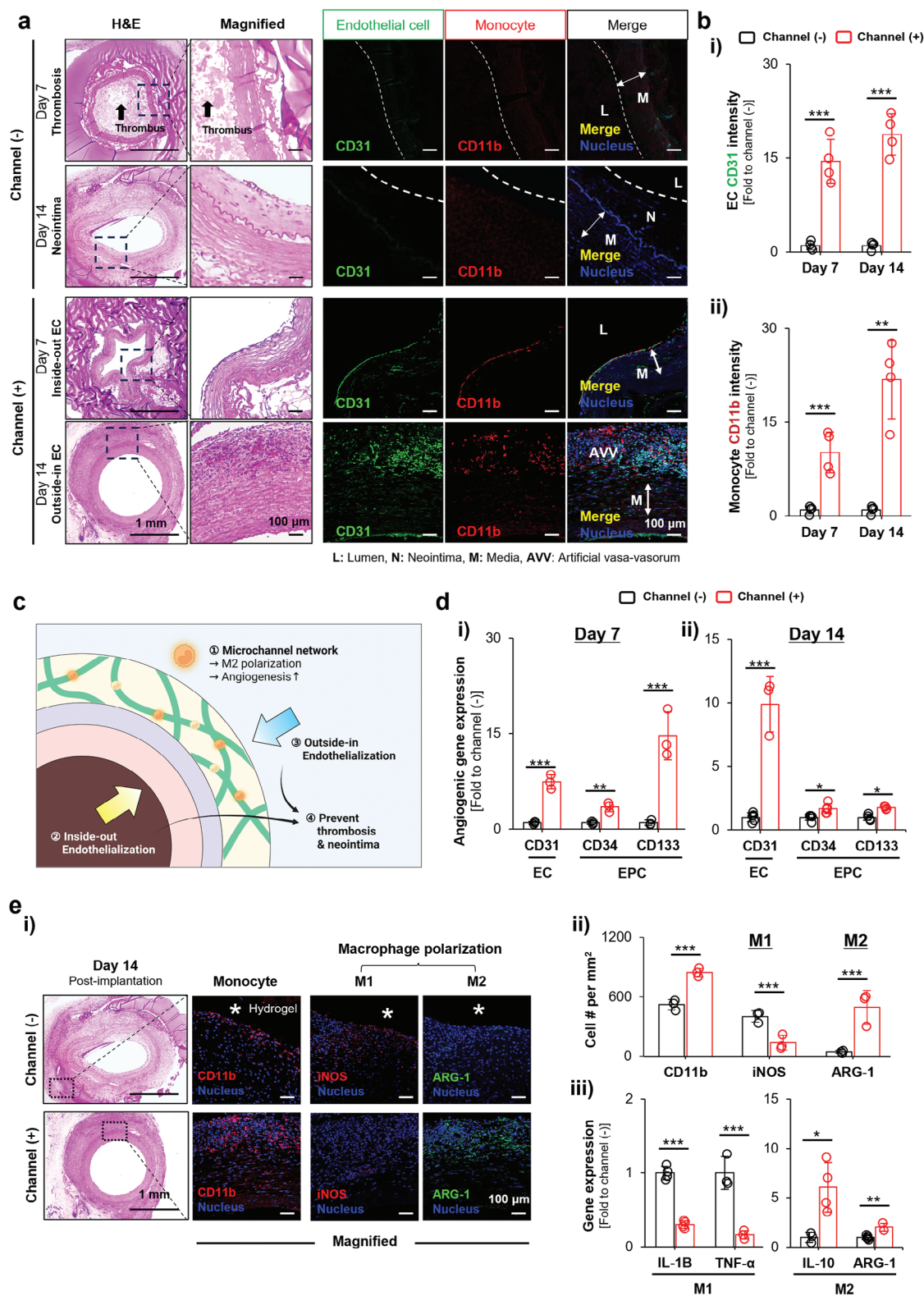


Figure 4. Pro-endothelialization by AVV through regenerative macrophage polarization. a) The channel (-) group induces thrombosis (Day 7) and neointima formation (Day 14) without endothelialization (CD31) and monocyte invasion (CD11b), which are prevented by AVV with endothelialization and monocyte invasion from the lumen to intima (inside-out, day 7) and from AVV on adventitia to media (outside-in, day 14) as b) confirmed by quantitative intensity analyses of i) CD31 and ii) CD11b expression. c) The overarching hypothesis is that EPCs are recruited from the luminal blood to intima (inside-out) first, and then, ECs invade through AVV on adventitia to media (outside-in). As a result, thrombosis and neointima formation are prevented

mechanism of vascular regeneration. Because the mechanism affects cellular restoration and repair in a layer-by-layer fashion throughout the cell-free vessel wall, AVV is suggested as a meaningful solution for vascular regeneration in agreement with the outside-in control paradigm. Moreover, the microchannel network physically drives the morphological change of macrophages as a decision-maker, indicating that the 3D AVV structure can guide a series of cellular responses in a cause-and-effect manner. Hence, this study presents a real model of a multi-disciplinary approach to translate engineering technology to the clinical side by controlling the biological mechanisms following the theme of structure-function relationship.

The development of small vascular grafts (< 6 mm diameter) has been an unmet subject despite extensive research for decades. The biomechanical properties of the graft play a crucial role in maintaining vascular patency. In this regard, the mismatched compliance around anastomotic sites generates blood shear gradients with consequent flow disturbance and platelet activation, which leads to thrombosis and graft failure.^[28] As a promising solution to overcome the mechanical mismatches, the material properties have been tuned using expanded polytetrafluoroethylene (ePTFE),^[29] polycaprolactone (PCL), polyurethane (PU), poly(L-lactide-co-ε-caprolactone) (PLCL), chitosan, and silk fibroin.^[30] Although these materials possess advantages regarding the customization of biomechanical properties in addition to easy availability, their long-term performance is limited due to the lack of vascular wall composition and structure. Hence, decellularized vessels have been considered as an alternative following the concept of allograft because the ECM composition and structure are at least preserved. However, despite these positive aspects, recellularization has been still considered as a challenge in moving toward clinical translation.^[31] Continuous progress has been made in improving the re-cellularization methodology using biocompatible materials and manufacturing techniques.^[32] The key point of successful regeneration is to restore the intact tissue structure and cellular composition like the native vessels. A variety of decellularized xenografts have been tested for clinical applications of arteriovenous access [e.g., Artegraft (bovine carotid artery), SynerGraft (bovine ureter), etc.]. However, unsatisfactory outcomes are reported concerning side effects such as thrombosis and aneurysm.^[33] Similar vascular grafts are made using porcine small intestinal submucosa (SIS), such as CorMatrix, resulting in stenosis of small-diameter vessels.^[34] Along the same line, the low patency resulted from the cell-free scaffold-only group without AVV support (Figure S5, Supporting Information). When the lessons of trials are considered, the present study approaches a simple but impactable strategy as the decellularization method is tuned to preserve the ECM composition including collagen and GAG. AVV induces restoration of cellular composition by preventing thrombosis through heparin immobilization like setting up the smart software to the well-structured

hardware. This study also reveals that vascular elasticity can be recovered after the restoration of vascular smooth muscle cells (VSMCs), which takes more than 4 weeks as a remodeling time. AVV plays a key role in these versatile regeneration processes by operating the inflammatory mechanism to facilitate VSMC restoration in addition to anti-thrombosis.

The three rabbit models are designed to represent the clinical needs in replacement and bypass grafting of small-diameter vessels so that the utilities of cell-free graft with AVV can be validated toward clinical translation for the three major cases of surgical treatment.^[35] As the coronary artery (diameter: 1–3 mm) and low extremity peripheral artery (diameter: < 1 mm) are prone to occlusion remodeling upon pathogenesis, the replacement grating is often considered the first choice of surgical treatment. In particular, the interposition model of the femoral artery requires difficult reconstructive microsurgery,^[36] while the aorto-iliac bypass model (diameter: > 3 mm) is approached using invasive and risky means to treat the above-knee peripheral artery disease and to mediate organ transplantation.^[37] The availability of size-matched grafts limits surgical success because the mismatched size results in flow disturbance and consequent graft failure. Moreover, as veins are usually used to graft into arteries, the mismatched mechanical properties add more issues that limit surgical efficacy. Hence, the present approaches in the three models indicate a promising option to match the size and arterial properties of the major grafting cases. Furthermore, bypass grafting is susceptible to bifurcative changes in the flow parameters, which is more challenging than end-to-end grafting. In this regard, the maintenance of flow patency in the aortoiliac bypass model indicates an advanced surgical utility to address the abnormal changes in hemodynamics post-bypass grafting.

The grafting model of rabbit carotid artery demonstrates the effective regeneration of cell-free scaffold through endothelialization and SMC restoration by the AVV operation of mechanisms with inflammatory cells and stem cells as major players. The models of femoral artery and aorta bypass grafting were designed to validate the feasibility of diversifying the clinical utilities. In contrast to the carotid artery model, these two models are often stopped due to the ethical challenges including sudden death during the bypass surgery in addition to post-surgical limb paralysis due to incomplete micro-anastomosis. As these issues limit obtaining enough subjects, the same levels of in-depth analyses could not be performed beyond the demonstration of patency maintenance as a feasibility of the diverse surgical utilities. As a further study, large animal models (e.g., porcine and canine) should be scrutinized to promote surgical tolerance. Although the successful maintenance of patency is reported in the three models of small vessel grafting, further studies are needed to examine the long-term patency for more than years. The current study focuses on the AVV effect on cellular restoration with the application utility for different sizes (<1, 1–3, and >3 mm)

with synergistic support by M2 polarization of monocytes upon invasion. d) AVV promotes the marker gene expression of EC (CD31) and EPC (CD 34 and 133) compared to the channel (-) group. The CD 31 expression is dominantly promoted on day 14 in contrast to CD 133 on day 7. e) Compared to the channel (-) group, i) AVV promotes monocyte invasion (CD11b) with induction of M2 marker (ARG-1) as opposed to M1 marker (iNOS). These results are supported by quantitative analyses of ii) the number of each monocyte type and iii) the marker gene expression of M1 (IL-1b, TNF-α) and M2 (IL-10, ARG-1) polarization on day 14. All statistical analyses and p-values are determined using one-way ANOVA followed by Tukey's multiple comparison test (N = 4/ Figure 4a–b and N = 3/ Figure 4d–e) (*p < 0.05, **p < 0.01, ***p < 0.001). (Figure 4c created with Biorender.com).

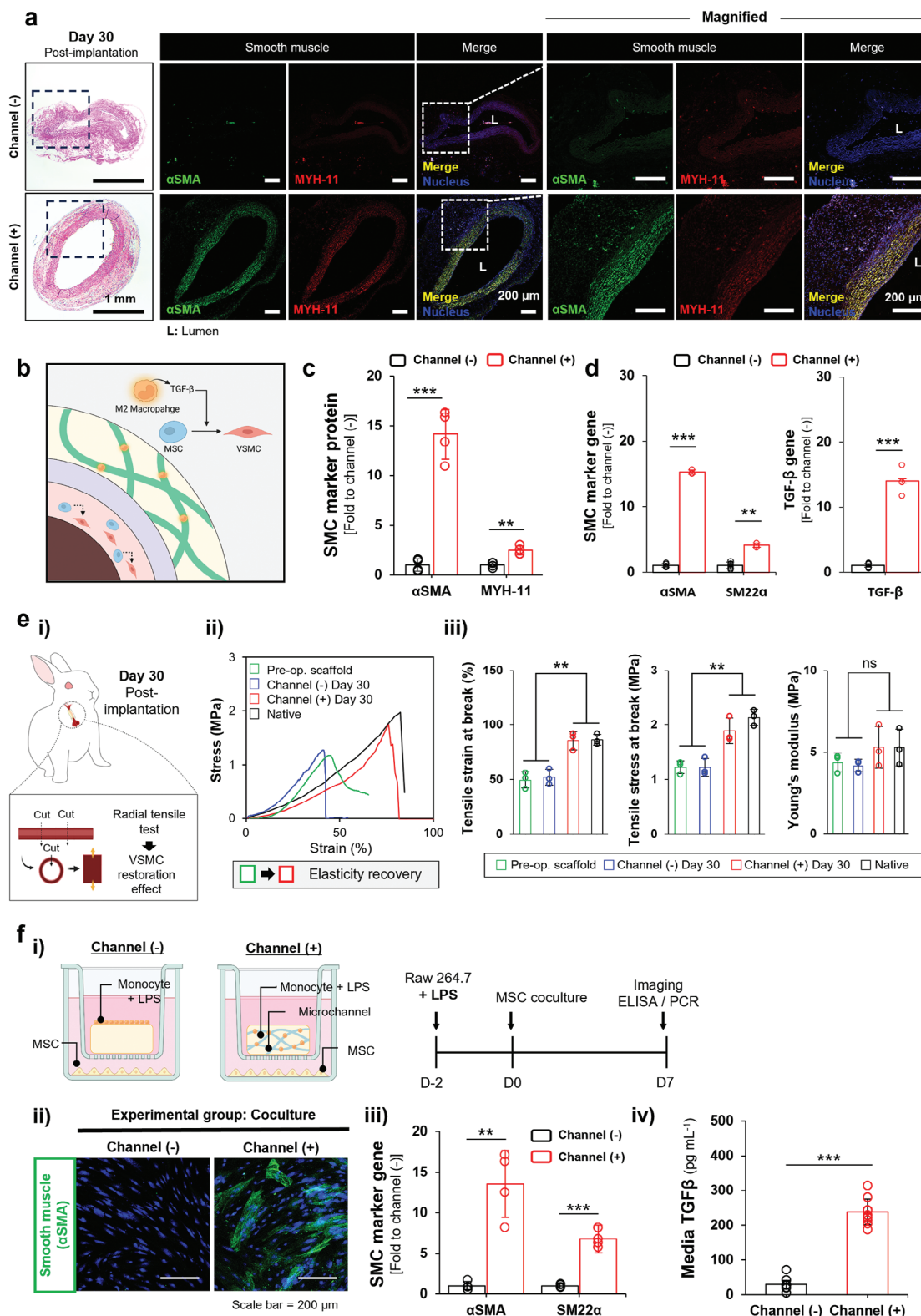


Figure 5. VSMC restoration by AVV through regenerative macrophage polarization. On day 30 post-implantation into a rabbit carotid artery, a) AVV promotes VSMC restoration into the tunica media of scaffold compared to the channel (-) group in H&E and immuno-staining (α SMA and MYH-11). b) AVV-induced M2 polarization of macrophages with consequent TGF- β production is proposed to drive the differentiation of perivascular MSCs to SMCs. c) This proposed mechanism is validated by the image analysis ($N = 4$, each group) with d) gene expression of α SMA, SM22 α , and TGF- β ($N = 3$, each group). e) i) In the radial tensile test of the harvested graft after tube cutting, ii) AVV increases the tensile stress and strain at break significantly

of vessel grafting. Thus, the endpoint analyses end up before the gel degradation is completed within a month. In addition to the known TGF- β effect, the key paracrine signals from the M2 polarization need to be determined through omics or systemic analyses in the next study because multi-way synergistic actions among the regenerative cytokine and growth factors are expected to involve SMC restoration.

Furthermore, the utility of AVV can be diversified beyond small vessel grafting to others including organoid implantation. Previous studies have demonstrated preservation of cell viability and functionality when spheroids or organoid cells are cultured in hydrogels with vascular structures.^[21] Along the same line, the present system enables circulatory anastomosis between the microchannel network and host vessels, suggesting the potential to produce artificial organs upon scaling up by embedding cells and tissues using the benefit of AVV function in addition to organoid implantation. Nonetheless, this study approaches a variety of new experiment models to validate the AVV function as the most challenging point, thereby generating new insight to guide a series of future studies.

4. Conclusion

The study highlights the control function of vascular out-wall for the regeneration of cell-free vessels by revealing the leading role of vasa vasorum in facilitating reciprocal interactions between the luminal and adventitial sides. Following this outside-in control paradigm, AVV is engineered by generating the densely interconnected microchannel networks within an implantable hydrogel. The catalytic role of AVV in operating the regenerative mechanism is validated through a series of clinically prevalent models of vascular grafting. The cell-free scaffold is prepared by decellularizing rabbit carotid arteries through comparative validation of methods to preserve the ECM composition with arterial mechanical properties, followed by wrapping the adventitia with AVV. In the rabbit models of inter-positional and bypass grafting, the AVV graft serves as an onsite recruiter of vascular cells to the cell-free wall by inducing M2 polarization of macrophages upon AVV channel-mediated packing in alignment. As a result, smooth muscle cells are restored with revitalization of vascular elasticity and the vascular patency is maintained effectively, suggesting a promising solution of small diameter vessel grafting.

5. Experimental Section

The Cell-Free Scaffold Harvested from Rabbit Arteries: The rabbit study was approved by the Institutional Animal Care and Use Committee (IACUC) of Yonsei University College of Medicine (authorization number #2021-0048). Rabbits (3 kg, male, New Zealand White) were purchased from Doo Yeol Biotech (Seoul, Republic of Korea) and acclimated to an animal facility for 1 week before use. Each rabbit was anesthetized through

intramuscular injection of zoletil (50 mg kg⁻¹, ZoletilTM, Virbac Korea, Seoul, Republic of Korea) and xylazine (5 mg kg⁻¹, Rompun, Bayer Korea, Seoul, Republic of Korea), followed by euthanasia via intravenous injection of potassium chloride (20 mg kg⁻¹, Choongwae Pharma Corporation, Seoul, Republic of Korea). After euthanasia, a midline incision was made into the neck skin, and branches of the right carotid artery were ligated using 9-0 sutures (Ethicon, Raritan, NJ, USA), followed by cross-clamping on the proximal and distal sides of the artery. A 5-cm segment of the carotid artery was excised, then gently washed with sterilized PBS to remove intravascular thrombus, and stored at 4 °C for late uses. The euthanized rabbits were also subjected to harvest of femoral artery and aorta for femoral artery interposition and aorta to iliac artery bypass surgeries, respectively. The carotid arteries were decellularized by either mechano-chemical [freeze-thaw cycling with 1% Triton X-100 (93 443, Sigma-Aldrich, St. Louis, MO, USA)] or chemico-chemical^[38] [1% sodium dodecyl sulfate (SDS; L3771, Sigma-Aldrich) with 1% Triton X-100 (Sigma-Aldrich)] method. Briefly, the mechano-chemical method was proceeded by freezing and thawing the artery at -80 °C and 37 °C for 30 mins, respectively with repetitions 10 times, followed by treatment with 1% Triton X-100 at 37 °C for 30 mins. In contrast, the chemico-chemical process was carried out by treating the artery with 1% SDS for 48 h and then with 1% Triton X-100 at 37 °C for 12 h. The decellularized arteries were defined as cell-free scaffolds; washed with distilled water; and sterilized by treating with 0.4% peracetic acid (269 336, Sigma-Aldrich) and 70% EtOH for 30 mins each, followed by PBS washing and lyophilizing (7 960 041, Labconco, KS, USA).

Fabrication of Artificial Vasa-Vasorum (AVV): A custom-built mold was created using polydimethylsiloxane (PDMS; Dow Corning, Midland, MI, USA) with the dimension of 3 (width) × 5 (depth) × 1 (height) cm, and then, a tubular space of 6 (diameter) mm × 4 (length) cm was obtained by casting a cylinder with curing. A silicone tube with an artery size of 2 (diameter) mm × 5 (length) cm was placed in the center of the cylinder space inside the mold. As a thermo-sensitive polymer, poly(N-isopropyl acrylamide) (pNIPAM; Mw = ≈40 000, Sigma-Aldrich) was used to produce a thread of sacrificial fibers as the means to generate microchannel networks. The pNIPAM powder was dissolved in methanol (53% w/v), which was subjected to fiber spinning at 2500–2800 rpm using a customized device as reported previously.^[20b,21,39] A tread of microfibers in 20–30 μm diameter was obtained and evenly placed around the silicone tube in the cylinder space of the PDMS mold. Then, gelatin and microbial transglutaminase (mTG) were mixed (9:1 ratio) in a PBS (5% w/v), which was poured into the cylinder space to cover the fibers and silicone tube, followed by mTG crosslinking reaction at 37 °C. Next, the pNIPAM microfibers were dissolved from mTG hydrogel through sol-gel transition, followed by immersing and perfusing with cold PBS (4 °C). In this way, channel networks were generated in the mTG gel as a form of AVV upon the replacement of a silicone tube with a cell-free scaffold. The pore generation within the mTG gel post-removal of sacrificial microfibers was visualized by scanning electron microscopy (SEM; MERLIN, Zeiss Merlin, Oberkochen, BW, Germany).

Tissue Staining: The samples were fixed with 4% paraformaldehyde (PFA) in PBS at 4 °C for 1 day, washed with PBS 3 times, paraffin-embedded, and cross-sectioned into 5 μm thickness. Hematoxylin and eosin (H&E) staining was performed following standard procedures, and the samples were examined by optical microscopy (DMI8M; Leica, Wetzlar, Germany). Immunofluorescence staining was conducted on the tissue slices after deparaffinizing with xylene and rehydrating in ethanol through a series of incubations (100%, 95%, 80%, 70% v/v in distilled water). Antigens were retrieved by heating the slides in citrate buffer (1X, pH 6.0, C9999, Sigma-Aldrich) for 30 mins at 95 °C, followed by inacti-

up to the native artery ii) compared to the other two groups. There is no significant difference in Young's modulus among the test groups ($N = 3$, each group). f) i) The mechanistic channel effect is determined by placing the channel (+) versus (-) hydrogels on the upper trans-well chamber (D-2) with Raw264.7 culture under LPS induction for 2 days. MSCs are cultured at the bottom of the well (D0) for 7 days to determine differentiation to SMCs by immunostaining, PCR, and ELISA. ii) The channel promotes α SMA expression in MSCs compared to the channel (-) group in the images as supported by iii) the expression of α SMA and SM22 α genes with iv) TGF- β production ($N = 5$, each group). Statistical analysis is carried out through one-way ANOVA with Tukey's multiple comparison test (ns: non-specific, $**p < 0.01$, $***p < 0.001$). (Figure 5b created with Biorender.com).

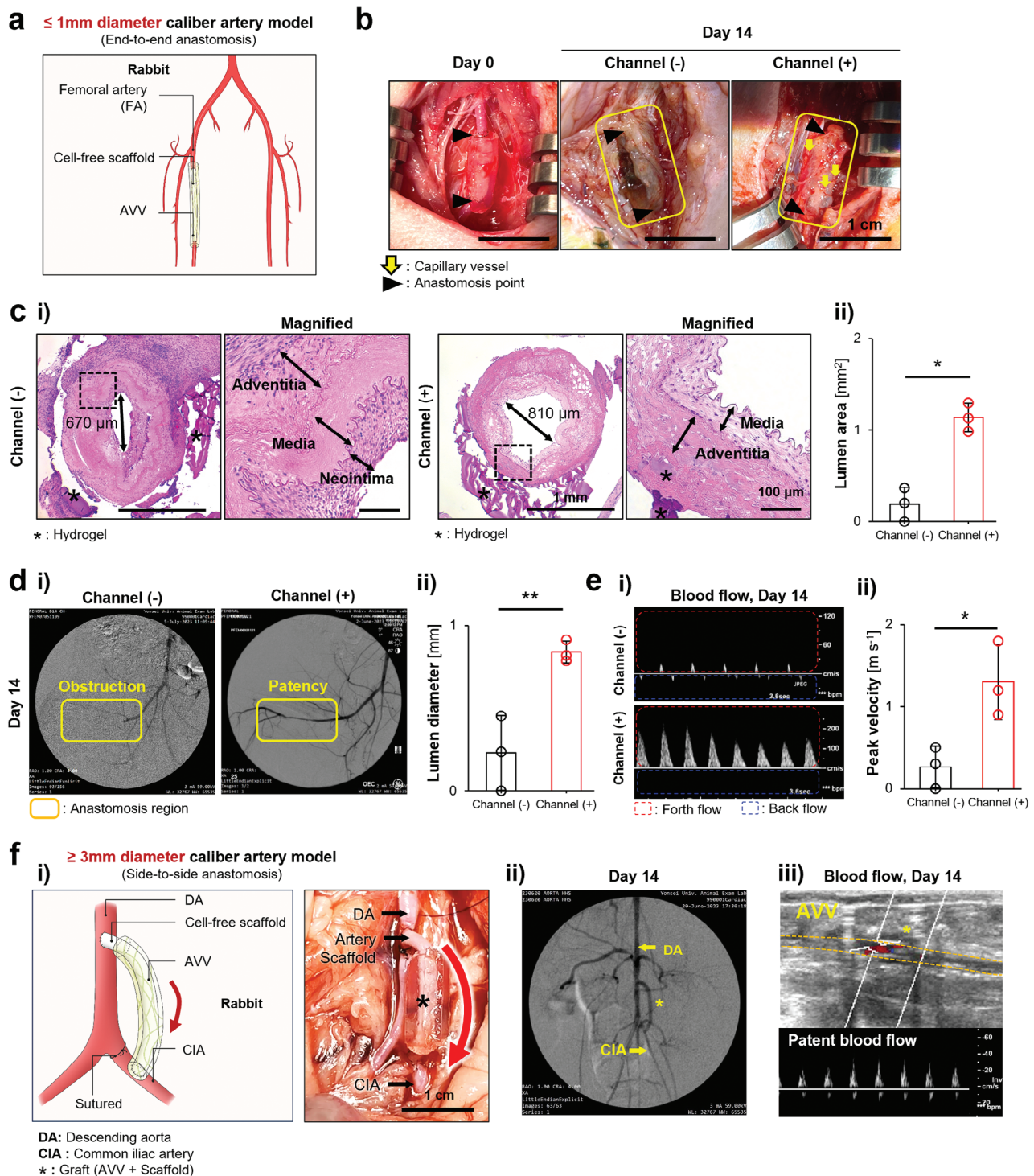


Figure 6. Effective AVV grafting to vessels in ≤ 1 or ≥ 3 mm diameter. a) As a microsurgical model for vessel replacement, the graft is interposed into a rabbit femoral artery (≤ 1 diameter) below the knee through end-to-end anastomosis. During 14 day-implantation, b) the successful grafting (day 0) undergoes micro-vascularization by AVV in contrast to the thrombotic colorization of the channel (-) group. c) AVV prevents i) neointima formation as opposed to the channel (-) group in the H&E staining images and ii) with agreement by the quantitative analysis of the lumen area. Compared to the channel (-) group, d) AVV i) promotes the graft patency with ii) the significant increase of lumen diameter in angiography, e) thereby generating i) the healthier flow patterns as supported by ii) the higher peak velocity under Doppler US. f) As a bypass grafting model for target vessels in ≥ 3 mm diameter, i) the AVV graft (AVV + scaffold) is subjected to side-to-side anastomosis with bypassing from the descending aorta to the common iliac artery (CIA). On day 14 post-implantation of the graft, ii) the flow patency is maintained clearly in angiography, iii) as evidenced further by the health pattern of high-peak pulsatile flow with a normal forward-to-backward ratio under Doppler US. All statistical and p-value analyses are performed using two-sided *t*-tests. (**p* < 0.05, ***p* < 0.01) (*N* = 3, each group). (Figure 6a, f created with Biorender.com).

vation of endogenous peroxidases using 3% H₂O₂ solution for 10 mins. Then, permeabilization was carried out by incubating with 0.1% Triton X-100 for 1 h, followed by washing. The samples were blocked with 5% bovine serum albumin (BSA; 82-100-6, Millipore, Burlington, MA, USA) in Tris-Buffered Saline, 0.1% Tween 20 detergent (TBST; Tech and Innovation, Chuncheon-si, Gangwon-do, Republic of Korea) at room temperature for 2 h. The samples were treated with primary antibodies against CD31 (1:100, NB600-562, Novus Biologicals LLC, Centennial, CO, USA), CD11b (1:100, LS-B3760, LS Bio, Seattle, WA, USA), α SMA (1:100, NB300-678, Novus Biologicals LLC), ARG-1 (1:200, LS-C447907, LS Bio), and/or iNOS (1:200, GTX17504, Genetex, Irvine, CA, USA), MYH-11 (1:200, NBP2-44532, Novus Biologicals LLC), CD90 (1:200, ab133350, Abcam, Cambridge, UK) overnight at 4 °C. After PBS washing, samples were incubated with secondary antibodies including anti-rabbit Alexa Fluor 488 and 594 (1:1000, 111-545-003 and 111-585-003, Jackson Immuno Research, West Grove, PA, USA), anti-goat Alexa Fluor 488 (1:1000, A11055, Invitrogen, Carlsbad, CA, USA), and/or anti-mouse Alexa Fluor 594 for 2 h in the dark. Nuclei were counterstained with NucBlue Live Ready Probes Reagent (R37605, Invitrogen), followed by confocal imaging (LSM 780, Zeiss, Oberkochen, Land Baden-Württemberg, Germany) with quantitative analyses using ImageJ (Fiji, National Institute of Health, MD, USA). Endothelialization of vasa-vasorum was determined through optical imaging of rabbit carotid arteries and grafts with subsequent treatment of CD31 primary antibodies as described above. The samples were then treated with HRP-labeled secondary antibodies (anti-mouse polymer, k4001; Agilent Dako) at RT for 20 mins. The samples were treated with DAB development solution (k3468; Agilent Dako) for 5 mins and washed with deionized water, followed by counterstaining with hematoxylin (k8008; Agilent Dako) and optical imaging.

Quantification of DNA and Sulfated(s) GAG: Both native and decellularized arteries were washed with PBS twice, freeze-dried, and digested by papain solution (76 216, Sigma-Aldrich) at 60 °C for 6 h. The lysates were used to determine the amounts of double-stranded DNA (dsDNA) content using the Quant-iT PicoGreen dsDNA assay kit (P11496, Thermofisher, Waltham, MA, USA). The lysate samples were mixed with the Quant-iT PicoGreen reagent and then subjected to fluorescence reading at 480 nm (excitation) and 520 nm (emission) using a fluorescence microplate reader (Varioskan Flash 3001, Thermofisher). The sGAG content of each lysate was quantified by a Blyscan™ Glycosaminoglycan Assay Kit (Biocolor, County Antrim, UK) according to the manufacturer's instructions. Briefly, the 1,9-dimethyl methylene blue cationic dye was reacted with the sGAG in the lysate solution, which was centrifuged for 30 mins at 14 000 rpm and resuspended using a dye-dissociated buffer. Then, the absorbance was measured at 656 nm in a microplate reader.

Western Blot: After storing in PBS at −20 °C, the arteries were minced using scissors and tissue homogenizer (Tissuextractor II, QIAGEN, Hilden, Germany) in RIPA buffer (R0278, Thermofisher) with 1X protease inhibitor (78 833, Thermofisher). The protein content of each lysate was quantified using the Bradford assay (B6916, Sigma-Aldrich). Then western blotting was carried out to analyze the expression of vascular proteins. Gel electrophoresis was performed using 10% SDS-polyacrylamide gels (10% w/v, 4 561 094, Bio-rad, Hercules, CA, USA), and the proteins were transferred onto a nitrocellulose membrane (IB23001, Thermofisher). The membrane was then blocked with 5% nonfat dry milk (1 706 404, Bio-rad) in 0.5% Tween-20 TBST solution and incubated with target primary antibodies for 24 h at 4 °C. Primary antibodies included β -actin (1:200, SC-47778, Santa Cruz Biotechnology, Dallas, TX, USA), CD31 (1:100, NB600-562, Novus Biologicals LLC), α SMA (1:100, MA5-11547, Invitrogen), and Type 1 collagen (1:1000, NB600-408, Novus Biologicals LLC). After washing, the membrane was reacted with secondary antibodies conjugated to HRP. Secondary antibodies included goat anti-rabbit antibody (1:1000, 31 460, Thermofisher) and goat anti-mouse antibody (1:1000, 31 430, Thermofisher). Chemiluminescence signals were visualized using a clarity western ECL substrate (1 705 060, Bio-rad), and the signals were captured using a gel documentation system (ImageQuant LAS 4000, GE Healthcare Life Sciences, Chicago, IL, USA).

Mechanical Test: Circumferential tensile properties of vessel samples were characterized to analyze i) changes in the mechanical properties

through the decellularization processes and ii) the elasticity restoration by smooth muscle regeneration after 1 month-implantation. Arteries were sectioned into rings and subjected to the tensile test immediately after surgery to minimize property alterations. The artery rings were cut in the vertical direction into the flattened, rectangular shape uniformly in 5 (width) \times 7 (length) mm. The tensile strength and Young's modulus of arteries and scaffolds were measured by DMA (DMA 850, TA instrument Inc. New Castle, DE, USA) under 10% min^{−1} of strain rate at 37 °C.

Perfusion and Diffusion Test: The microchannel network of gel was stained by perfusing microbead (0.1 μ m, Invitrogen). The perfusion and diffusion efficiencies of microchannel networks in AVV were then tested by perfusing microbeads (2 μ m, Invitrogen) and diffusing Fluorescein Isothiocyanate (FITC)-dextran (40 kDa, Sigma-Aldrich). As in vitro samples, gels (+/- microchannel network) were prepared with embedding silicone tube (I.D. = 1 mm, O.D. = 2 mm, SL-0102, LK LAB Korea, Gyeonggi-do, Republic of Korea) as a model of cell-free scaffold. The silicone tube was connected by a straight connector (30622-49, SCIST, Donginbio, Seoul, Republic of Korea). As in vivo samples, the grafts were harvested after 30-day implantation into a rabbit carotid artery through interposition surgery. The straight connector was attached to the end of each scaffold using a 4-0 silk suture (Ethicon) without any leak. Then, a syringe pump (LEGATO210, KdScientific, Holliston, MA, USA) was used to perfuse red microbeads (1:5000 in PBS) at a rate of 20 μ L min^{−1} or FITC-dextran (0.1% w/v in PBS) was diffused into the gels through an inlet connector under confocal imaging (LSM 980, Zeiss). Colormaps were visualized using ImageJ software (Fiji), followed by quantitative analysis using MATLAB software (Mathworks, Natick, MA, USA).

Heparin Immobilization with Platelet Tests: Heparin was immobilized onto the cell-free scaffolds through the reaction of 1-ethyl-3-(3-dimethyl aminopropyl) carbodiimide (EDC; E1769, Sigma-Aldrich) and N-hydroxysuccinimide (NHS; 130 672, Sigma-Aldrich). Briefly, heparins (2000 I.U., JW Pharmaceutical Corporation, Seoul, Republic of Korea), EDC (120 mmol L^{−1}), and NHS (60 mmol L^{−1}) were reacted in 2-(N-morpholino) ethanesulfonic acid buffer (MES; 0.1 M, pH 6.0, Biosolution, Seoul, Republic of Korea) for 30 mins at room temperature to activate carboxylic acid groups of heparins. The pH of the solution was adjusted to 8–9 using NaOH, followed by scaffold immersion for 4 h at room temperature with continuous shaking. After washing with DI water, the amount of immobilized heparin in each scaffold was determined by staining with 1 mL of Toluidine blue O solution (TBO; T3260, Sigma-Aldrich) containing 0.1 M HCl at room temperature for 4 h,^[40] followed by DI water washing for 24 h to remove residual TBO solution. Then, the samples were dissolved in a mixture of 0.1 M NaOH and ethanol (1:4, volume ratio) until complete decolorization and subjected to absorbance reading at 530 nm in a microreader.

The heparin immobilization was verified by testing platelet adhesion and activation on the scaffolds. Blood was extracted from the right marginal ear vein of the rabbit using a 20G butterfly needle and collected in sodium citrate tubes (369 714, BD Bioscience, Becton, NJ, USA). The blood solution was centrifuged at 3000 rpm at 4 °C for 10 mins, and then, only the platelet-poor plasma and buffy coat layer were transferred to new sample tubes. Subsequently, the samples were centrifuged at 2500 rpm at 4 °C for 5 mins, and the platelet-rich plasma in the upper layer was carefully collected. The scaffolds (+/- heparin immobilization) were reacted with platelets in PBS dilution at 37 °C for 1 h, followed by PBS washing twice, fixing with 2% glutaraldehyde in PBS for 6 h, and dehydration in Critical Point Dryer (EM CPD300, Leica, Austria). The adhesion and activation of platelets on the test scaffolds were visualized using an SEM with quantitative image analyses using ImageJ (Fiji).

Arterial Grafting Models in Rabbits: All animal experiments utilized cell-free scaffolds after decellularization using the mechano-chemical method with subsequent heparin immobilization. The cell-free scaffolds were generated using the carotid artery, femoral artery, or aorta for the corresponding model of interposition or bypass grafting to minimize the mismatch of vessel diameters between the host and graft vessels. To prevent thrombosis on the grafts after implantation, aspirin (5 mg kg^{−1}, Bayer, Leverkusen, Germany,) was administered orally into each rabbit from day 3 before surgery until day 14 post-surgery. Each rabbit was anesthetized through

a subcutaneous injection of 10 mg kg⁻¹ zoletil, and anesthesia was maintained with endotracheal inhalation of isoflurane (2–2.5%, Hana Pharm, Gyeonggi, Republic of Korea). As a model of the central small artery (1–1.5 mm in diameter), a carotid artery of each rabbit was subjected to surgical interposition with the graft. The rabbits of the carotid interposition model were divided into three groups: the cell-free scaffold-only group without hydrogel (N = 4), with hydrogel without channel [channel (-), N = 15], and with hydrogel and channel [channel (+), N = 15]. A 4-cm incision was made at the center anterior neck so that the carotid artery was exposed through dissection of the subcutaneous tissue and neck muscle. The branches of the carotid artery were tied to block blood flow using 9-0 ethilon sutures, followed by an intravenous injection of heparin (100 IU kg⁻¹, JW Pharmaceutical, Seoul, Republic of Korea). Then, both proximal and distal sides of the artery were clamped using micro-devices (JD-S-101MC, Jeung Do Bio, Seoul, Republic of Korea), and the arterial segment between the clamps was excised. The graft (2 cm in length) was inserted into the segment spot with end-to-end anastomosis using a 9-0 ethilon suture, and the neck soft-tissue was closed using a 4-0 vicryl suture, followed by skin closure using 4-0 ethilon suture.

As a model of the peripheral small vessel (< 1 mm in diameter), a femoral artery of each rabbit was subjected to surgical interposition with the graft by starting to make a linear incision (4 cm) on the inner thigh. Then, the femoral artery, vein, and nerve bundle were identified by exposing the gracilis muscle around the superficial side of the thigh. The proximal and distal sides of the artery were clamped using a micro-device so that the artery between the clamps was excised, followed by interposing the graft through an end-to-end anastomosis using a 10-0 prolene suture.

Lastly, the graft was bypassed from the aorta to the iliac artery graft by starting to make a linear incision (7–8 cm) along the mid-line of the abdomen so that the abdominal cavity was exposed by dissecting the muscles and fascia. Gauzes were soaked in warm saline and placed in the cavity to prevent hypothermic injury and tissue dehydration during surgery. Next, the retroperitoneal space around the aorta bifurcates and the iliac arteries were identified by careful dissection. Then, the proximal aorta and the distal side of the right and left iliac arteries were clamped, followed by bypass grafting through side-to-side anastomosis with the aorta and through end-to-end anastomosis with the iliac artery using 9-0 Ethilon sutures. Soft tissues and skin were closed using a 4-0 vicryl and 4-0 ethilon suture, respectively. Each group started with 15 rabbits for the grafting surgery of the carotid artery. Then, the five rabbits in poor conditions with arterial occlusion under Doppler US imaging were subjected to endpoint analyses at the earlier time point. The other rabbits were kept in the progress to the further time points. The healthy group underwent random selections to match the number of animals (N = 5) between the groups at each time point.

After the surgeries, the rabbits were carefully monitored daily for 30 days, with pain control by administering meloxicam (0.5 mg kg⁻¹, Medica Korea, Seoul, Republic of Korea) orally once a day for the first 7 days. Infection was prevented through oral administration of enrofloxacin (10 mg kg⁻¹, CTBio Inc., Hwaseong-si, Gyeonggi-do, Republic of Korea) for the first 7 days. The rabbits were euthanized using a bolus intravenous injection of potassium chloride (20 mg kg⁻¹; Choongwae Pharma Corporation) under general anesthesia, and tissue samples at the surgical sites were then harvested for analysis.

Angiography and Doppler Sonography: Ultrasonography (iU22 xMatrix DS, Philips, Amsterdam, Netherlands) was carried out to examine blood flow profiles on day(s) 0 (right after grafting), 7, 14, and 30 (N = 5 for each group). The blood flow was analyzed using color Doppler and pulse wave (PW) modes. Angiography was performed on the carotid and femoral arteries (day 30) and the bypass graft (day 14) using C-arm x-ray equipment (General Electric, NY, USA). First, the vessel (non-surgical site) was exposed by making an incision, followed by inserting a 4 Fr sheath (TERUMO, Seoul, Republic of Korea) into the vessel. Next, a 0.014-inch guidewire (Asahi Intecc Medical, Tokyo, Japan) was introduced through the sheath to the target site, and a 4 Fr catheter was positioned near the target site following the guidewire path. Contrast media (Scal-nux, SANOCHEMIA, Austria) were mixed with normal saline (1:1 ratio,

Choongwae Pharma Corporation), which was injected into the catheter to acquire vessel images.

Cell Culture: Raw264.7 cell (ATCC, Manassas, VA, USA), human endothelial progenitor cell (EPC; Cellprogen, Benelux, Netherlands), and human mesenchymal progenitor cell (hMSC; Lonza, Basel, Switzerland) were purchased without any ethical issues. Raw264.7 cells were cultured using Dulbecco's modified Eagle's medium (DMEM)-High glucose (11995-065, Gibco, Carlsbad, CA, USA) supplemented with 10% fetal bovine serum (FBS; 16000-044, Gibco) and 1% penicillin-streptomycin (PS; 15140-122, Gibco). hMSCs were cultured using DMEM-Low glucose (11885-084, Gibco). EPCs were cultured using progenitor cell complete media with serum (M36081-13S, Cellprogen, Torrance, CA, USA) following the manufacturer's manual. Each cell type was propagated until 80% confluency was reached and then detached using 0.25% trypsin/ethylenediaminetetraacetic acid (Trypsin/EDTA; Gibco) for subculture.

Human induced pluripotent stem cells were reprogrammed to endothelial cells (hiPSC-EC) as reported previously⁴⁰ and cultured in mTeSR 1 medium (85 850, STEMCELL Technologies, Vancouver, Canada) on 5% Matrigel (354 277, Corning, NY, USA)-coated plates at 37 °C with 5% CO₂. The medium was exchanged daily until 95% cell confluency was reached in a 100 mm dish, followed by detaching hiPSC-ECs with Phosphate Buffered Saline (PBS; Welgene, Gyeongsangbuk-do, Republic of Korea) containing 0.5 mM EDTA. Then, the cells were transferred to an anti-attachment tube using mTeSR 1 medium and 5% Matrigel, which was coated onto an ultra-low attachment Petri dish (100 mm). The culture medium containing 5% Matrigel was changed daily for 3 days on a shaker at 37 °C with 5% CO₂. After enzymatic dissociation, clumps of hiPSCs (passages < 60) were differentiated to ECs by culturing on 0.01% collagen-coated plates in DMEM/F12 medium supplemented with 20% serum replacement and specific differentiation factors for 10 days.

iPSC-EC as an EPC Model to Recruit by AVV: As an EPC model, iPSC-ECs were embedded into the gelatin/mTG solution (1 × 10⁷ cells mL⁻¹), which was used to produce the graft samples with AVV or (-) channel. These samples were exposed to a closed circulation of culture media by perfusing into the inlet silicone tube in connection with the graft samples. Then, iPSC responses were examined under the perfusion and diffusion of media with or without the microchannel networks of AVV. An arterial flow was generated at a continuous rate of 346.9 µL min⁻¹ using a peristaltic pump (BT100-1L-A, Baoding Longer Precision Pump, Hebei, China) for 7 days. The graft samples were fixed in 4% PFA at 4 °C for 1 day and washed three times with PBS, followed by cell permeabilization using 0.3% Triton X-100 in PBS at room temperature for 1 h. After washing with PBS three times, cell viability was determined using the Live/DEAD Viability/Cytotoxicity Kit (L3324, Invitrogen) by incubating samples with 4 mM calcein-AM (live-green) and 2 mM ethidium homodimer-1 (dead-red) for 30 minutes in the culture media. After counterstaining nuclei with DAPI (R37606, ThermoFisher) at room temperature for 20 minutes, the samples were subjected to confocal imaging (LSM 980, Zeiss) for qualitative and quantitative image analyses of viable endothelialization into the samples.

In Vitro Macrophage Polarization: Gel samples (5% w/v +/- channel network) were prepared in a disc size of 1 cm (diameter) × 2 mm (thickness). Raw264.7 macrophages (ATCC, 1 × 10⁶ cells) were cultured onto each hydrogel sample in a high-glucose DMEM medium for 2 days. Then, macrophages were activated by treating with 1 µg mL⁻¹ of lipopolysaccharide (LPS; Sigma-Aldrich) for 7 days, followed by fixing with 4% PFA for 24 h. The samples were permeabilized with 0.1% Triton X-100 in PBS and blocked with 5% BSA at room temperature for 2 h. Macrophage polarization was determined by immunofluorescent staining with sample treatment using primary antibodies against ARG-1 (M2 marker, 1:100, NBPI-43347, Novus Biologicals LLC) and iNOS (M1 marker, 1:100, GTX17504, Genetex, Irvine, CA, USA) overnight at 4 °C. The samples were washed and incubated with secondary antibodies for 2 h in the dark, followed by nucleus counterstaining with NucBlue Live Ready Probes Reagent (Invitrogen) and confocal imaging (LSM 780, Zeiss).

In Vitro EPC Migration by Macrophage Polarization in AVV: Raw264.7 cells (ATCC, 1 × 10⁶ cells mL⁻¹) were embedded into gelatin hydrogels (0.5 cm diameter and 2 mm thickness +/- channel network) as described

above and cultured in the media for 3 days. Then, the macrophages were activated by LPS ($1 \mu\text{g mL}^{-1}$) treatment (day 0) and used to determine EPC migration by M2 polarization of macrophages due to the microchannel effect. Following the manufacturer's instruction, the radius migration assay (CBA-125, Cell Biolabs, San Diego, CA, USA) was carried out by seeding EPCs (2×10^5 cells per well) in specialized 24-well plates (112 501, Cell Biolabs). The center (diameter 0.68 mm) of the well was coated with a biocompatible radius gel. After culturing the EPCS for 24 h, the center gel was removed using a gel removal solution (112 504, Cell Biolabs), thereby generating a cell-free circular region. Then, the gel samples with activated macrophages were placed on the cell-free region and subjected to a 14-day culture, followed by determining EPC migration toward the cell-free region. After removing the hydrogel samples, EPCs were fixed with 4% PFA for 24 h and treated using Alexa488-labeled F-actin (A12379, Thermofisher), followed by nucleus staining with NucBlue Live Ready Probes Reagent (Invitrogen) and confocal imaging (LSM780, Zeiss) with quantitative image analysis using ImageJ (Fiji).

In Vitro VSMC Restoration by Macrophage Polarization in AVV: Because AVV was proposed to induce M2 polarization of macrophages with TGF- β production, hMSCs were used as a precursor cell type of VSMCs to determine the TGF- β effect on the direction of differentiation by qRT-PCR and immunostaining. Gels (+/- channel network) with a disc size [1 cm (diameter) \times 2 mm (thickness)] were prepared. Raw264.7 macrophages were seeded onto the gels in a 6-well culture plate (1×10^6 cells mL^{-1}) and cultured for 48 h. Then, the gels were treated with LPS ($1 \mu\text{g mL}^{-1}$, Sigma-Aldrich) for macrophage activation and placed in the top chamber of the trans-well plate (0.4 μm in pore diameter, 35 006, SPL, Gyeonggi-do, Republic of Korea). Then, hMSCs (5×10^5) were seeded onto the bottom chamber to co-culture for 7 days. The amount of TGF- β was determined using ELISA by obtaining the supernatant from the upper chamber media. The samples were fixed at 4% PFA, permeabilized with 0.25% Triton X-100 solution, blocked, washed, and incubated with the primary antibody (αSMA ; 1:1000, Abcam) at 4 $^{\circ}\text{C}$ for 24 h with PBS washing. The fluorescent-labeled secondary antibody (Alexa Fluor 488 Goat anti-Mouse; 1:1000, Thermo Fisher) was then applied to the samples for 2 h at room temperature, followed by confocal imaging (LSM 780, Zeiss) with quantitative analysis using ImageJ (Fiji).

ELISA: The TGF- β ELISA kit (88-8350-88, Thermofisher) was used following the manufacturer's instructions. A 96-well plate (9018, Corning, USA) was coated with the capture antibodies by incubating overnight at 4 $^{\circ}\text{C}$, which was blocked with ELISA/ELISPOT (00-4202-56, Thermofisher) at room temperature for 1 h. Recombinant TGF- β was used to generate a standard curve through 2-fold serial dilutions to reach 8 points. Latent TGF- β in the supernatant of co-culture media was converted into an immunoreactive form through acid activation by treating with 1N HCl, followed by neutralization with 1N NaOH. The co-culture supernatants (100 μL) were added to the wells with sealing and incubated at room temperature for 2 h or overnight at 4 $^{\circ}\text{C}$ to increase the sensitivity. Next, the detection antibodies were added to the wells and incubated at room temperature for 1 h, followed by incubating with Avidin-HRP at room temperature for 30 mins. The fluorescence intensity was measured at 450 nm by subtracting the background value (570 nm) using a microplate reader.

Quantitative RT-PCR: Target marker genes were identified to determine M1 (IL-1 β , iNOS, TNF α , IL-6) and M2 (CD206, CD163, IL-10, ARG-1, TGF- β) polarization of macrophages, SMC phenotype (αSMA and SM22 α), and angiogenesis (CD31, CD34, CD133). Total RNA was extracted using an RNA extraction kit (74 106, Qiagen, Hilden, Germany), following the manufacturer's protocol. The RNA concentration was determined using a Nanodrop 2000 spectrophotometer (ND2000, Thermofisher). Complementary DNA (cDNA) was synthesized through reverse transcription using the AccuPower CycleScript RT premix (K2044, Bioneer). Real-time PCR (StepOne V2.3, Applied Biosystems, MA, USA) was conducted using cDNA, SYBR green (Applied biosystems), and primers (Cosmo Genetech, Seoul, Republic of Korea). The PCR program was set for 40 cycles of target gene amplification with a holding stage at 95 $^{\circ}\text{C}$ for 10 mins, denaturation at 95 $^{\circ}\text{C}$ for 1 min, and annealing at 60 $^{\circ}\text{C}$ for 1 min. Glyceraldehyde 3-phosphate dehydrogenase (GAPDH) was

used as a housekeeping gene, and relative gene expression was analyzed using the $2^{-\Delta\Delta\text{Ct}}$ method.

Data Analysis: All experimental data were presented as mean \pm standard deviation (SD), and the n number of samples was denoted in each figure legend. These samples were obtained from more than three independent experiments and represented with dots and whisker plots as the average and minimum/maximum values, respectively. The unpaired Student's t-test was used for pairwise comparisons, and a one-way analysis of variance (ANOVA) was utilized for multiple-group comparisons. Post-hoc analyses including Tukey's method were used to determine group-wise differences. Significance levels were indicated by p-values ($*p < 0.05$, $**p < 0.01$, and $***p < 0.001$). All statistical analyses were conducted using Excel, SigmaPlot (V12.0, Systat Software Inc., San Jose, CA, USA), MATLAB, and GraphPad Prism 5 (San Diego, CA, USA). Quantitative image analyses including color image processing were carried out using ImageJ software (Fiji).

Supporting Information

Supporting Information is available from the Wiley Online Library or from the author.

Acknowledgements

H.-S.H., S.B., and K.L. contributed equally to this work. This work was supported by the Korean Fund for Regenerative Medicine (KFRM) grant funded by the Korean government (the Ministry of Science and ICT, the Ministry of Health & Welfare) (KFRM 23A0203L1) with support from the MD-PhD/Medical Scientist Training Program through the Korea Health Industry Development Institute (KHIDI) in the Ministry of Health and Welfare.

Conflict of Interest

The authors declare no conflict of interest.

Data Availability Statement

The data that support the findings of this study are available from the corresponding author upon reasonable request.

Keywords

artificial vasa-vasorum, cell-free artery, macrophage polarization, microchannel network, small vessel graft

Received: December 1, 2023
Revised: February 4, 2024
Published online: March 10, 2024

- [1] a) M. Lovett, K. Lee, A. Edwards, D. L. Kaplan, *Tissue Eng., Part B* **2009**, 15, 353; b) C. O'Connor, E. Brady, Y. Zheng, E. Moore, K. R. Stevens, *Nat. Rev. Mater.* **2022**, 7, 702.
- [2] a) K. Hu, Y. Li, Z. Ke, H. Yang, C. Lu, Y. Li, Y. Guo, W. Wang, *Biomaterials Translational* **2022**, 3, 81; b) N. Méndez-Barbero, C. Gutiérrez-Muñoz, L. M. Blanco-Colio, *Int. J. Mol. Sci.* **2021**, 22, 7284; c) M. R. Bennett, S. Sinha, G. K. Owens, *Circ. Res.* **2016**, 118, 692.
- [3] a) H. W. Kim, H. Shi, M. A. Winkler, R. Lee, N. L. Weintraub, *Arterioscler., Thromb., Vasc. Biol.* **2020**, 40, 2569; b) M. J. Mulligan-Kehoe, M. Simons, *Circulation* **2014**, 129, 2557; c) M. W. Majesky, X. R. Dong, V. Högglund, W. M. Mahoney Jr, G. Daum, *Arterioscler., Thromb., Vasc. Biol.* **2011**, 31, 1530.

- [4] V. Musil, J. Sach, D. Kachlik, M. Patzelt, J. Stingl, *Surgical and Radiologic Anatomy* **2018**, *40*, 1159.
- [5] J. A. Phillippi, *Sci. Adv.* **2022**, *8*, eabl6364.
- [6] A. Loesch, M. R. Dashwood, *Journal of Cell Communication and Signaling* **2018**, *12*, 631.
- [7] F. Y. McWhorter, C. T. Davis, W. F. Liu, *Cell. Mol. Life Sci.* **2015**, *72*, 1303.
- [8] G. Cao, X. Xuan, J. Hu, R. Zhang, H. Jin, H. Dong, *Cell Commun. Signaling* **2022**, *20*, 1.
- [9] A. M. Malek, S. L. Alper, S. Izumo, *JAMA, J. Am. Med. Assoc.* **1999**, *282*, 2035.
- [10] Y. Tai, E. L. Woods, J. Dally, D. Kong, R. Steadman, R. Moseley, A. C. Midgley, *Biomolecules* **2021**, *11*, 1095.
- [11] a) H. Ha, C. H. Lee, K. S. Lee, K. Lee, J. Park, S. Y. Kim, S. Baek, M. L. Kang, D. W. Lee, H. J. Sung, *Small* **2023**, *19*, 2303325; b) A. M. Ross, Z. Jiang, M. Bastmeyer, J. Lahann, *Small* **2012**, *8*, 336.
- [12] a) T. J. Barrett, *Arterioscler., Thromb., Vasc. Biol.* **2020**, *40*, 20; b) M. K. Khoury, H. Yang, B. Liu, *Arterioscler., Thromb., Vasc. Biol.* **2021**, *41*, e77.
- [13] a) J. Rehman, J. Li, C. M. Orschell, K. L. March, *Circulation* **2003**, *107*, 1164; b) F. Lopes-Coelho, F. Silva, S. Gouveia-Fernandes, C. Martins, N. Lopes, G. Domingues, C. Brito, A. M. Almeida, S. A. Pereira, J. Serpa, *Cells* **2020**, *9*, 107.
- [14] A. Kumar, S. S. D'Souza, O. V. Moskvina, H. Toh, B. Wang, J. Zhang, S. Swanson, L.-W. Guo, J. A. Thomson, I. I. Slukvin, *Cell Rep.* **2017**, *19*, 1902.
- [15] a) B. C. Isenberg, C. Williams, R. T. Tranquillo, *Circ. Res.* **2006**, *98*, 25; b) S. Fang, D. G. Ellman, D. C. Andersen, *Cells* **2021**, *10*, 713.
- [16] a) L. Niklason, J. Gao, W. Abbott, K. Hirschi, S. Houser, R. Marini, R. Langer, *Science* **1999**, *284*, 489; b) C. B. Weinberg, E. Bell, *Science* **1986**, *231*, 397.
- [17] S. Pashneh-Tala, S. MacNeil, F. Claeysens, *Tissue Eng., Part B* **2016**, *22*, 68.
- [18] H. Yuan, C. Chen, Y. Liu, T. Lu, Z. Wu, *J. Biomed. Mater. Res., Part A* **2020**, *108*, 426.
- [19] X. Wang, V. Chan, P. R. Corridon, *Frontiers in Bioengineering and Biotechnology* **2022**, *10*, 951644.
- [20] a) J. B. Lee, D.-H. Kim, J.-K. Yoon, D. B. Park, H.-S. Kim, Y. M. Shin, W. Baek, M.-L. Kang, H. J. Kim, H.-J. Sung, *Nat. Commun.* **2020**, *11*, 615; b) S. J. Yoon, S. Baek, S. E. Yu, E. Jo, D. Lee, J. K. Shim, R. J. Choi, J. Park, J. H. Moon, E. H. Kim, *Adv. Healthcare Mater.* **2022**, *11*, 2201586.
- [21] J. B. Lee, J. S. Park, Y. M. Shin, D. H. Lee, J. K. Yoon, D. H. Kim, U. H. Ko, Y. Kim, S. H. Bae, H. J. Sung, *Adv. Funct. Mater.* **2019**, *29*, 1900075.
- [22] Y. Huo, T. Luo, J. M. Guccione, S. D. Teague, W. Tan, J. A. Navia, G. S. Kassab, *PLoS One* **2013**, *8*, e73769.
- [23] M. A. Rodriguez-Soto, N. Suarez Vargas, A. Riveros, C. M. Camargo, J. C. Cruz, N. Sandoval, J. C. Briceño, *Cells* **2021**, *10*, 3140.
- [24] T. L. Akentjew, C. Terraza, C. Suazo, J. Maksimcuka, C. A. Wilkens, F. Vargas, G. Zavala, M. Ocaña, J. Enrione, C. M. García-Herrera, *Nat. Commun.* **2019**, *10*, 3098.
- [25] A. A. Szklanny, M. Machour, I. Redenski, V. Chochola, I. Goldfracht, B. Kaplan, M. Epshtein, H. Simaan Yameen, U. Merdler, A. Feinberg, *Adv. Mater.* **2021**, *33*, 2102661.
- [26] M. M. De Santis, H. N. Alsafadi, S. Tas, D. A. Bölükbas, S. Prithiviraj, I. A. Da Silva, M. Mittendorfer, C. Ota, J. Stegmayr, F. Daoud, *Adv. Mater.* **2021**, *33*, 2005476.
- [27] F. Y. McWhorter, T. Wang, P. Nguyen, T. Chung, W. F. Liu, *Proc. Natl. Acad. Sci. USA* **2013**, *110*, 17253.
- [28] W. S. Nesbitt, E. Westein, F. J. Tovar-Lopez, E. Tolouei, A. Mitchell, J. Fu, J. Carberry, A. Fouras, S. P. Jackson, *Nat. Med.* **2009**, *15*, 665.
- [29] C. Li, A. Hill, M. Imran, *J. Biomater. Sci., Polym. Ed.* **2005**, *16*, 875.
- [30] a) G. Soldani, P. Losi, M. Bernabei, S. Burchielli, D. Chiappino, S. Kull, E. Briganti, D. Spiller, *Biomaterials* **2010**, *31*, 2592; b) S. Fang, A. H. Ahlmann, L. Langhorn, K. Hussein, J. A. Sørensen, X. Guan, S. P. Sheikh, L. P. Riber, D. C. Andersen, *Regener. Med.* **2021**, *16*, 117; c) C. S. Ong, T. Fukunishi, R. H. Liu, K. Nelson, H. Zhang, E. Wiecek, M. Palmieri, Y. Ueyama, E. Ferris, G. E. Geist, *Tissue Eng., Part C* **2017**, *23*, 728; d) P. Gupta, B. B. Mandal, *Acta Biomater.* **2021**, *134*, 79.
- [31] L. Gui, A. Muto, S. A. Chan, C. K. Breuer, L. E. Niklason, *Tissue Eng., Part A* **2009**, *15*, 2665.
- [32] D. Durán-Rey, V. Crisóstomo, J. A. Sánchez-Margallo, F. M. Sánchez-Margallo, *Frontiers in bioengineering and biotechnology* **2021**, *9*, 771400.
- [33] C.-H. Lin, K. Hsia, H. Ma, H. Lee, J.-H. Lu, *Int. J. Mol. Sci.* **2018**, *19*, 2101.
- [34] N. Hibino, P. McConnell, T. Shinoka, M. Malik, M. Galantowicz, presented at Seminars in thoracic and cardiovascular surgery, **2015**.
- [35] S. Fang, D. Ellman, D. Andersen, *Cells* **2021**, *10*, 713.
- [36] B. O. Mofikoya, A. O. Ugboro, O. B. Bankole, *Journal of hand and microsurgery* **2011**, *3*, 15.
- [37] Y. Ünlü, P. Keleş, S. Keleş, H. Yeşilyurt, H. Koçak, S. Diyarbakırlı, *Surg. Today* **2003**, *33*, 725.
- [38] J. S. Lee, J. Shin, H.-M. Park, Y.-G. Kim, B.-G. Kim, J.-W. Oh, S.-W. Cho, *Biomacromolecules* **2014**, *15*, 206.
- [39] J. B. Lee, D.-H. Kim, J.-K. Yoon, D. B. Park, H.-S. Kim, Y. M. Shin, W. Baek, M.-L. Kang, H. J. Kim, H.-J. Sung, *Nat. Commun.* **2020**, *11*, 1.
- [40] J.-O. Jeong, S. I. Jeong, J.-S. Park, H.-J. Gwon, S.-J. Ahn, H. Shin, J. Y. Lee, Y.-M. Lim, *RSC Adv.* **2017**, *7*, 8963.